Pole-to-pole validation of Envisat GOMOS ozone profiles using data from ground-based and balloon sonde measurements

Y. J. Meijer, D. P. J. Swart, M. Allaart, S. B. Andersen, G. Bodeker, I. Boyd, G. Braathen, Y. Calisesi, H. Claude, V. Dorokhov, et al.

Pole-to-pole validation of Envisat GOMOS ozone profiles using data from ground-based and balloon sonde measurements

Y. J. Meijer,[1,2] D. P. J. Swart,[1] M. Allaart,[3] S. B. Andersen,[4] G. Bodeker,[5] I. Boyd,[5,6] G. Braathen,[7] Y. Calisesi,[8] H. Claude,[9] V. Dorokhov,[10] P. von der Gathen,[11] M. Gil,[12] S. Godin-Beekmann,[13] F. Goutail,[14] G. Hansen,[15] A. Karpetchko,[16] P. Keckhut,[17] H. M. Kelder,[2,3] R. Koelemeijer,[18] B. Kois,[19] R. M. Koopman,[20] G. Kopp,[21] J.-C. Lambert,[22] T. Leblanc,[23] I. S. McDermid,[23] S. Pal,[24] H. Schets,[25] R. Stubi,[26] T. Suortti,[16] G. Visconti,[27] and M. Yela[12]

Received 30 March 2004; revised 30 July 2004; accepted 20 September 2004; published 9 December 2004.

[1] In March 2002 the European Space Agency (ESA) launched the polar-orbiting environmental satellite Envisat. One of its nine instruments is the Global Ozone Monitoring by Occultation of Stars (GOMOS) instrument, which is a medium-resolution stellar occultation spectrometer measuring vertical profiles of ozone. In the first year after launch a large group of scientists performed additional measurements and validation activities to assess the quality of Envisat observations. In this paper, we present validation results of GOMOS ozone profiles from comparisons to microwave radiometer, balloon ozonesonde, and lidar measurements worldwide. Thirty-one instruments/launch sites at twenty-five stations ranging from the Arctic to the Antarctic joined in this activity. We identified 6747 collocated observations that were performed within an 800-km radius and a maximum 20-hour time difference of a satellite observation, for the period between 1 July 2002 and 1 April 2003. The GOMOS data analyzed here have been generated with a prototype processor that corresponds to version 4.02 of the operational GOMOS processor. The GOMOS data initially contained many obviously unrealistic values, most of which were successfully removed by imposing data quality criteria. Analyzing the effect of these criteria indicated, among other things, that for some specific stars, only less than 10% of their occultations yield an acceptable profile. The total number of useful collocated observations was reduced to 2502 because of GOMOS data unavailability, the imposed data quality criteria, and lack of altitude overlap. These collocated profiles were compared, and the results were analyzed for possible dependencies on several geophysical (e.g., latitude) and GOMOS observational (e.g., star characteristics) parameters. We find that GOMOS data quality is strongly dependent on the illumination of the limb through which the star is observed. Data measured under bright limb conditions, and to a certain extent also in twilight limb, should be used with caution, as their usability is doubtful. In dark limb the GOMOS data agree very well with the correlative data, and between 14- and 64-km altitude their differences only show a small (2.5–7.5%)

[1]Laboratory for Environmental Measurements, Environmental Risks and Safety Division, National Institute of Public Health and the Environment, Bilthoven, Netherlands.
[2]Also at Faculty of Applied Physics, Eindhoven University of Technology, Eindhoven, Netherlands.
[3]Royal Netherlands Meteorological Institute, De Bilt, Netherlands.
[4]Danish Meteorological Institute, Copenhagen, Denmark.
[5]National Institute of Water and Atmospheric Research, Lauder, New Zealand.
[6]Department of Astronomy, University of Massachusetts, Amherst, Massachusetts, USA.
[7]Norwegian Institute for Air Research, Kjeller, Norway.
[8]Institute of Applied Physics, Bern, Switzerland.
[9]Deutscher Wetterdienst, Hohenpeissenberg, Germany.
[10]Central Aerological Observatory, Moscow, Russia.
[11]Alfred Wegener Institute for Polar and Marine Research, Potsdam, Germany.
[12]Instituto Nacional de Técnica Aeroespacial, Torrejon de Ardoz, Spain.
[13]Centre National de la Recherche Scientifique, Paris, France.
[14]Centre National de la Recherche Scientifique, Verrieres-le-Buisson, France.
[15]Norwegian Institute for Air Research, Tromsø, Norway.
[16]Finnish Meteorological Institute, Sodankylä, Finland.
[17]Institut Pierre Simon Laplace, Université de Versailles Saint-Quentin, Verrieres-le-Buisson, France.
[18]Netherlands Environmental Assessment Agency, Bilthoven, Netherlands.
[19]Institute of Meteorology and Water Management, Warsaw, Poland.
[20]European Space Agency, Frascati, Italy.
[21]Institut für Meteorologie und Klimaforschung, Forschungszentrum Karlsruhe, Karlsruhe, Germany.
[22]Space Aeronomy Institute of Belgium, Brussels, Belgium.
[23]Jet Propulsion Laboratory, Wrightwood, California, USA.
[24]Meteorological Service of Canada, Toronto, Ontario, Canada.
[25]Royal Meteorological Institute of Belgium, Brussels, Belgium.
[26]MeteoSwiss, Payerne, Switzerland.
[27]Department of Physics, University of L'Aquila, L'Aquila, Italy.

0148-0227/04/2004JD004834

insignificant negative bias with a standard deviation of 11–16% (19–63 km). This conclusion was demonstrated to be independent of the star temperature and magnitude and the latitudinal region of the GOMOS observation, with the exception of a slightly larger bias in the polar regions at altitudes between 35 and 45 km. *INDEX TERMS:* 0365 Atmospheric Composition and Structure: Troposphere—composition and chemistry; 0394 Atmospheric Composition and Structure: Instruments and techniques; 3360 Meteorology and Atmospheric Dynamics: Remote sensing; 3394 Meteorology and Atmospheric Dynamics: Instruments and techniques; *KEYWORDS:* GOMOS, Envisat, ozone profile, validation, stratosphere, remote sensing

Citation: Meijer, Y. J., et al. (2004), Pole-to-pole validation of Envisat GOMOS ozone profiles using data from ground-based and balloon sonde measurements, *J. Geophys. Res.*, *109*, D23305, doi:10.1029/2004JD004834.

1. Introduction

[2] The declining stratospheric ozone layer, the changing global climate and the increasing pollution of the troposphere have created a growing public concern regarding the impact of human activities on the Earth's atmosphere. In the past two decades researchers in various scientific disciplines have made considerable efforts to try to understand the underlying chemical and physical processes and the role of anthropogenic gas emissions. The catalytic destruction of stratospheric ozone due to the presence of chlorine compounds and the role of greenhouse gases in the Earth's radiation budget were soon identified and ultimately led to international policy responses, such as the Montreal and Kyoto protocols. The further monitoring of the effect of these protocols and the impact of human activities on the atmosphere is of great importance, and relies critically on the availability of various key atmospheric state parameters.

[3] In March 2002 the European Space Agency (ESA) launched the polar-orbiting environmental satellite Envisat which is designed to provide measurements of not only the atmosphere, but also of the oceans, land and ice over a 5-year period. Previously, the Global Ozone Monitoring Experiment (GOME), on board the second European Remote Sensing (ERS-2) satellite, demonstrated the successful exploitation of European atmospheric chemistry instruments. GOME has been delivering global measurements of several key trace gases since its launch in 1995. Much longer records of the vertical distribution of ozone are provided by measurements of the Stratospheric Aerosol and Gas Experiment (SAGE) and Solar Backscatter Ultraviolet (SBUV) instruments [*McCormick et al.*, 1989; *Bhartia et al.*, 1996].

[4] Envisat incorporates three instruments measuring the lower and middle atmosphere. Making use of a variety of measurement techniques, these three instruments should significantly enrich the number of detectable species and their vertical distribution. The Michelson Interferometer for Passive Atmospheric Sounding (MIPAS) instrument is a Fourier transform spectrometer detecting the Earth's limb emission in the midinfrared. The Scanning Imaging Absorption Spectrometer for Atmospheric Chartography (SCIAMACHY) instrument is an ultraviolet–visible–near-infrared (UV-VIS-NIR) spectrometer allowing observations in nadir, limb emission and solar occultation mode. A third atmospheric instrument on board Envisat, the Global Ozone Monitoring by Occultation of Stars (GOMOS) instrument, is a medium-resolution stellar occultation spectrometer operating in the UV-VIS-NIR spectral range.

[5] A major contribution to the validation program of Envisat is provided by the principal investigators (PIs) of approved Announcement of Opportunity (AO) project proposals submitted to ESA. The joint activities of these AO projects and additional activities under direct contract, for the geophysical validation of Envisat's instruments, are performed in several subgroups of the Atmospheric Chemistry Validation Team (ACVT). The Ground-Based Measurement and Campaign Database (GBMCD) team, with the participation of a large number of organizations, institutes and individual scientists, forms the largest subgroup of the ACVT. Networks of ground-based instruments and sonde launch sites provide a suite of correlative measurements covering a wide range of geophysical conditions (i.e., latitude, longitude, season, altitude range, etc.). Apart from the few profiles of large-balloon and aircraft campaigns, all ozone profile data in the ACVT come from within the GBMCD subgroup resulting from the measurements performed by standard ozonesondes, ozone lidar systems, and microwave radiometer systems at many sites around the world. The extensive set of coincident data allows statistical analyses and investigation of relevant parameters.

[6] An initial geophysical validation campaign has been carried out during the Commissioning Phase of the mission (covering originally the first six months after launch, later extended to a total of 9 months). The preliminary validation results of this campaign were presented during the Envisat validation workshop from 9 to 12 December 2002 in Frascati, Italy [*European Space Agency* (*ESA*), 2003]. To enhance the clarity of quality statements and recommendations for possible improvements of each product, the analysis of each instrument's geophysical parameter had been centralized within the GBMCD subgroup. This paper forms a continuation and extension of the work presented by *Meijer et al.* [2003a] on the joint validation results of GOMOS ozone profiles. Here, significantly more GOMOS data will be analyzed compared to the study of *Meijer et al.* [2003a], which are from a longer period and correlate to more GBMCD sites, resulting in better statistics and allowing the study of additional (possible) dependencies.

[7] The main role of GOMOS will be the monitoring of trends and the observation of ozone in the stratosphere. Current instruments that measure stratospheric and mesospheric ozone profiles, including MIPAS and SCIAMACHY, either provide very accurate observations but with limited geographical coverage (e.g., SAGE), or good geographical

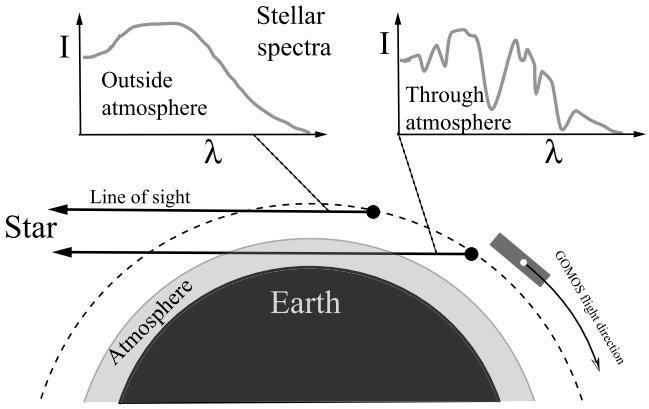

Figure 1. Illustration of the stellar occultation measurement principle, which is based on the changing spectrum of a light source when viewed outside and through the Earth's atmosphere.

coverage but with limited accuracy (e.g., GOME). GOMOS should strike an excellent compromise between these two extremes. The instrument is designed to supply accurate middle-atmosphere ozone abundances allowing precise monitoring of global ozone throughout the mission's lifetime. Optimum performance is expected to be achieved at altitudes between 15 and 80 km and under nighttime conditions, whereas the effective sensitivity is a function of brightness and spectral characteristics of the tracked target star.

[8] Many scientists will be able to exploit the different validated data products of Envisat and the synergy provided by the three atmospheric instruments. In this paper, we will provide the user community with an assessment of the quality of the ozone profiles retrieved from GOMOS observations by the processing algorithms of data processor version 4.02. In section 2 we introduce the measurement technique, the instrument and the data product of GOMOS. In section 3 we briefly present the origin and the measurement principles of the GBMCD correlative data including the applied criteria for collocation. In section 4 we discuss how we filtered GOMOS observations to select data of good quality, before comparing them with correlative data sets. In section 5 we show the analysis results of the comparison. In section 6 we give the conclusions and recommendations of the GOMOS ozone profile assessment.

2. GOMOS Data

[9] The GOMOS instrument exploits the stellar occultation technique for the detection of atmospheric ozone and other trace gases, as well as temperature [*Bertaux et al.*, 1991, 2004; *Kyrölä et al.*, 2004]. This technique allows the acquisition of spatially high-resolution atmospheric transmission spectra. Using these spectra and the known molecular cross sections, the vertical trace gas profiles are retrieved. The primary goal of GOMOS is the accurate detection of stratospheric ozone, allowing one to monitor global trends in this species over long periods. This section is subdivided into three parts and we initially present the stellar occultation principle, then the instrument design and finally the data product. Parts of this section have been adapted from ESA publications [*Ratier et al.*, 1999; *Nett et al.*, 2001; *ESA*, 2002].

2.1. Stellar Occultation Principle

[10] The occultation principle is based on the changing spectrum of a light source observed outside and through the Earth's atmosphere (Figure 1). Initially, the stellar (or solar) spectrum is measured when the star can be seen above the atmosphere. Subsequently, measurements are made viewing the star through the atmosphere providing spectra with absorption features from the passage through the atmosphere. The specific benefit of the occultation principle is its self-calibrating property, because when the spectra are divided by the spectrum measured outside the atmosphere, nearly calibration-free horizontal transmissions are obtained. Ozone profile information is embedded in the changing UV spectrum during, for example, a stellar occultation (Figure 2). The stellar occultation technique has previously been employed on the Midcourse Space Experiment (MSX) satellite using the Ultraviolet and Visible Imagers and Spectrographic Imagers (UVISI), and there have been several papers, both theoretical and applied, relating to these data [*Yee et al.*, 2002; *DeMajistre and Yee*, 2002; *Vervack et al.*, 2002, 2003; *Swartz et al.*, 2002]. UVISI and GOMOS specifically use stars as sources of light whereas other instruments have favored the Sun and/or the Moon. For example, the SAGE-I/II/III [*World Meteorological Organization* (*WMO*), 1988, pp. 52–65], the Stratospheric Aerosol Measurement (SAM-II), the Halogen Occultation Experiment (HALOE), the two Polar Ozone and Aerosol Measurement (POAM-II/III), the two Improved Limb Atmospheric Spectrometer (ILAS-I/II) and the SCIAMACHY instruments exploit the solar and/or lunar occultation technique. Note that the stellar occultations are done as star set observations, whereas solar occultations are done for both sunrise and sunset.

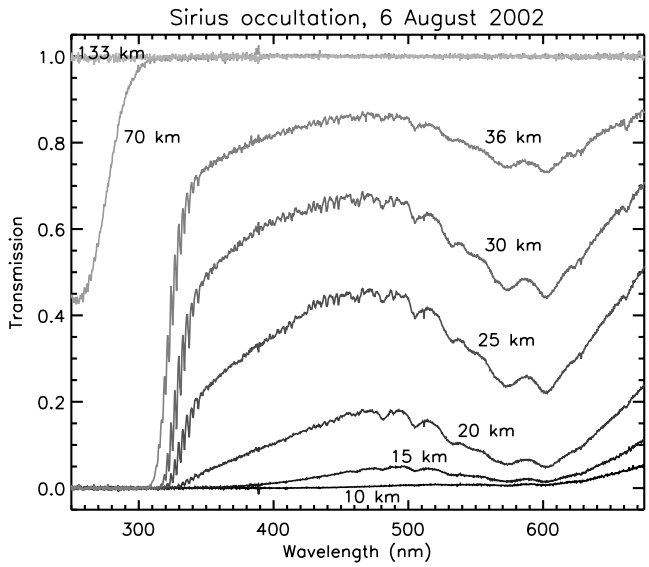

Figure 2. Example of GOMOS transmission spectra measured in flight at different tangent altitudes during an occultation of Sirius on 6 August 2002. The effect of the ozone absorption bands is clearly visible below 310 and around 600 nm.

[11] The specific advantages of the stellar occultation method are the good global coverage provided by the multitude of stars and the good altitude resolution (for GOMOS, typically 0.3–1.7 km) provided by the point source character of stars. There are also disadvantages, because the point source character of stars, and the weakness of their radiation, makes it necessary to consider some questions that are not relevant to solar occultations. A weak light source implies that additional light sources cannot be neglected, as they may compete with the desired stellar signal. For example, during half an orbit the limb is illuminated by the Sun, and therefore GOMOS will also detect scattered solar light, which usually dominates the observed signal. In addition, GOMOS will see light coming from auroral and other natural emissions in the atmosphere. A point source character implies that in the retrieval scheme special attention must be paid to the refractive effects on the propagation of stellar light through the atmosphere including, e.g., scintillation effects.

2.2. GOMOS Instrument

2.2.1. Design

[12] GOMOS tracks stars by using a large steerable mirror in front of the entrance telescope. The line of sight (LOS) between the instrument and the observed star can be pointed over a large contiguous range and is controlled by information provided by star trackers. The LOS can be pointed in azimuth from −10 to 90 degrees (with respect to the antiflight direction), and in elevation from 68 down to 62 degrees (with respect to the nadir direction). GOMOS is able to observe and track stars down to magnitude 4. A complex star-tracking system allows the star to be tracked within 20 μrad during the 50 s of a typical occultation scan. The star tracker is able to follow a star down to 15–25-km tangent altitude, which depends on the physical properties of a star, and the bright/dark atmospheric limb condition. Under optimal conditions, tracking down to 4-km tangent altitude has been achieved. The limb condition results from measurements made on either the day (bright) or night (dark) side of the orbit.

[13] Behind the mirror, a 20 × 30-cm^2 Cassegrain telescope simultaneously feeds two spectrometers and two photometers. For spectral measurements in the ozone Huggins and Chappuis bands, there is a medium-resolution (0.89 nm) spectrometer in the range 250–675 nm. There is a high-resolution (0.12 nm) spectrometer in the range 756–773 and 926–952 nm, for O_2 and H_2O measurements respectively. The two fast photometers, with a 1-kHz sampling rate, operate in the 470–520 nm and 650–750 nm spectral bands, for observing scintillation. Although GOMOS is specifically optimized for nighttime observations, it also performs measurements during daytime (bright limb conditions). Especially during daytime measurements, the background limb spectrum resulting from scattered solar light needs to be removed from the stellar spectra. For GOMOS this is solved by simultaneously measuring the pure limb signal just above and below the star LOS, and subtracting the interpolated spectrum from the stellar spectrum.

2.2.2. Star Selection and Mission Planning

[14] The stars used are those that provide a sufficient flux between 250 and 950 nm, which is the spectral range of interest for the target species, and hence where the GOMOS detectors and star tracking system are sensitive. The instrumental performance restricts the visual magnitudes to 4 or less and the acceptable (equivalent blackbody) temperature range to 3000–40,000 K. GOMOS measurements will obviously be difficult to interpret in case of rapidly varying stars, and difficulties will also be encountered if two or more stars are visually close to each other. The overall list of suitable target objects is a catalogue containing ∼1000 stars.

[15] Various simulations have been performed to determine the merit functions of different observing strategies. The selection of the stars and the optimization of the overall measurement sequence are performed on the ground for a series of orbits. This takes into account the various scientific objectives and ensures an even distribution of global measurements throughout the year. In this manner, the instrument typically acquires 40 stars per orbit, yielding ∼200,000 occultations per year. An example of the geographical coverage obtained after one month of GOMOS observations is shown in Figure 3. Inherent to the Sun-synchronous orbit of Envisat, the same star can be observed 14 times per day at different longitudes and more or less the same latitude, and in the course of the month also the latitude changes more clearly. The geographical coverage depends on the availability of suitable stars, which is of course varying as the Earth progresses in its orbit around the Sun. In 2003 the minimum and maximum observed latitude were −79.9 and 89.7, respectively.

2.3. Processing of Data Product

[16] First, the acquired transmission spectra are corrected for background limb radiation and scintillation effects. The scintillation correction is derived from the observed differences in scintillation between the two photometers, which observe in the blue and the red, and is based on the changing refractive index with wavelength [*Dalaudier et al.*, 2001; *Kan et al.*, 2001; *Bertaux et al.*, 2004]. The remaining transmittance can then be related to atmospheric constituent densities (O_3, NO_2, NO_3, O_2, H_2O, OClO, aerosol, and air density). Second, a spectral inversion is performed [*Kyrölä et al.*, 1993], which produces horizontal column densities of different constituents; i.e., the concentrations integrated along the LOS. Finally, a vertical inversion is performed [*Sihvola*, 1994], which converts the LOS column densities to vertical concentration profiles and can be conceptualized as a more sophisticated version of "onion peeling."

[17] Nominally the GOMOS data products should be generated and distributed by ESA's Envisat Payload Data Segment (PDS), which is their operational processing chain. Initially, the data could not be provided to the calibration and validation (Cal/Val) teams because of data generation and dissemination problems, and ESA has arranged for alternative data supply using the prototype processing chain at ACRI (Sophia Antipolis, France). During the Commissioning Phase, a strong sensitivity of the GOMOS detectors to radiation impact and additional unexpected phenomena affecting the retrieval have been detected. A major upgrade of algorithms has been implemented in several successive steps, and for this reason the supply of prototype data has been maintained, in order to allow Cal/Val teams to benefit from improved products at the earliest possible time, well ahead of implementation in the operational processors. The

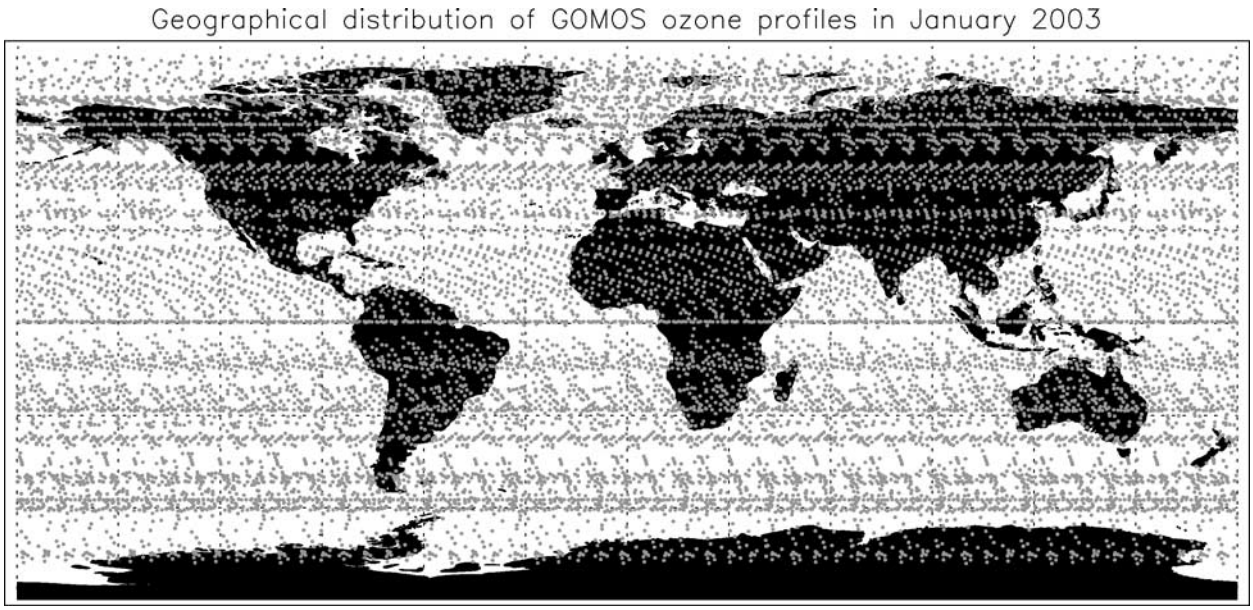

Figure 3. Geographical distribution of the geolocation (gray dots) of occultation measurements (~15,600) performed by GOMOS in January 2003. Inherent to the Sun-synchronous orbit of Envisat, the same star can be observed 14 times per day at different longitudes and more or less the same latitude, and in the course of the month the latitude also changes more clearly. The geographical coverage depends on the availability of stars, which, of course, varies as the Earth progresses in its orbit around the Sun.

data analyzed in this paper have been generated with the prototype processor in a version (GOPR_LV2_5.4b) equivalent to the version 4.02 (v4.02) of the operational (i.e., PDS) processor, which is the first GOMOS data version cleared for release to all GOMOS users.

[18] The product of interest for this paper is the vertical ozone profile given as number densities on geometric altitude levels. These data are provided together with several auxiliary parameters of which mainly the characteristics of the star used in the observation are important for the analysis. The star temperature and magnitude determine the signal strength of the observed UV spectrum, which influences the ozone retrieval. The hot and bright stars have a favorable signal to noise ratio and hence are expected to give better ozone profile accuracy, as shown in Figure 4 for different combinations of star temperature and visual magnitude. As will be demonstrated later, it is important to know whether the stellar signal was observed in a bright or dark background, but the current file output from the GOMOS processor (v4.02) does not yet contain information about the position of the Sun. Therefore we have calculated the solar zenith angle (SZA) with respect to the geolocation of the lowest tangent point (i.e., its latitude and longitude projected on the surface), and added this to the standard GOMOS data. In addition, the data product from this processor version does not contain the LOS azimuth angle at which a star is observed, and this information was obtained in a separate request to the processing unit at ACRI.

3. GBMCD Correlative Data

3.1. Introduction

[19] The Ground-Based Measurement and Campaign Database (GBMCD) subgroup of the ACVT provides data from ground-based instruments and small balloons to the central ACVT database for correlative measurements, which is maintained and facilitated by the Norwegian Institute for Air Research (NILU). For comparison to GOMOS ozone profiles, there are three different sources of correlative data available, and in the following three sections we briefly describe their observation techniques. In addition, in each section is explained how these data were converted to the same measurement units as the GOMOS data (i.e., ozone number density as a function of geometric altitude). Section 3.5 gives an overview of all contributions, which is followed by a discussion in section 3.6 on how to deal with data quality issues. In section 3.7 we explain the chosen criteria for the definition of a collocated measurement.

3.2. Ozonesonde Data

[20] The lower part of the atmosphere, between ground and 30-km altitude, is sampled by Electrochemical Concentration Cell (ECC) ozonesondes based on small balloons. These soundings are performed between 1 and 3 times per week as part of routine and special (validation) campaign observations. In the ECC sondes, air is pumped through a chemical cell containing an aqueous solution of potassium iodide [*Komhyr*, 1969; *Komhyr and Harris*, 1971]. The chemical reaction with ozone results in molecular iodine that can be detected and directly related to the ozone abundance in the outside air. Data are therefore provided as partial ozone pressure as a function of air pressure. The use of the ideal gas law and the assumption of hydrostatic equilibrium, which requires the additionally measured pressure and temperature information, yield the conversion to the common units for comparison. Some of the ozonesonde data used in this study were measured by a Brewer-Mast

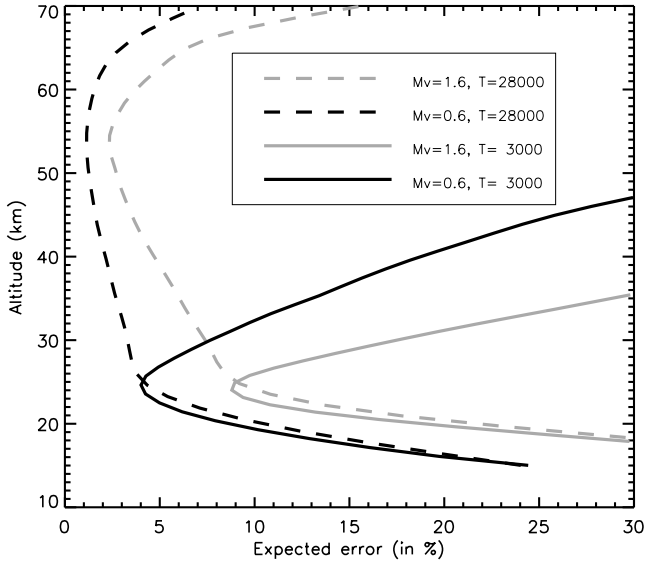

Figure 4. Simulation results of expected ozone profile accuracy for different combinations of star temperature T and visual magnitude M_v [*Ratier et al.*, 1999, Figure 6]. Dashed lines correspond to hot stars, whereas cold stars are indicated with solid lines. Gray and black correspond to examples using a weak and a strong star, respectively.

sonde, which mainly differs from the ECC sonde in the concentrations of the electrolyte and the design of the cell.

3.3. Stratospheric Ozone Lidar Data

[21] Stratospheric ozone lidar systems measure the atmosphere between about 15- and 50-km altitude. These measurements are performed between 1 and 3 times per week, which is dependent on weather and atmospheric conditions. Lidar systems are usually operated at night under clear-sky conditions, but some lidars have been adapted for daytime use in polar regions. Stratospheric ozone lidar instruments use a special lidar system, which is called a Differential Absorption Lidar (DIAL) system [*Measures*, 1984; *McDermid et al.*, 1990]. These systems simultaneously emit two light pulses at different wavelengths with different ozone absorption cross sections. The differences in light intensity backscattered from different altitudes can be directly related to the local ozone concentrations. Data are provided as ozone number densities as a function of geometric altitude and hence no conversion is necessary.

3.4. Microwave Radiometer Data

[22] Ozone in the stratosphere and mesosphere can be measured with microwave radiometers (MWRs). These measurements are performed almost continuously during both daytime and nighttime and are largely unaffected by clouds. These systems detect the microwave emissions of atmospheric ozone using a millimeter wave receiver and multichannel spectrometer [*Parrish et al.*, 1992]. In the observed spectrum ozone lines and their pressure-broadened shape can be used to reveal altitude-resolved ozone information, which is based on the optimal estimation technique of *Rodgers* [2000]. Data are provided as volume mixing ratios as a function of air pressure, and in addition these data come with averaging kernels and a priori information. The conversion to the common units is performed by assuming hydrostatic equilibrium and applying the ideal gas law, which requires the use of the provided pressure and temperature information.

3.5. Overview of Contributions

[23] In the period between 1 July 2002 and 1 April 2003 a large number of instruments at numerous measurement sites around the world have acquired an overwhelming amount of correlative data, sometimes as part of dedicated Envisat measurement campaigns. An overview of these instruments, stations and their details is provided in Table 1, which is sorted by geolocation (i.e., descending latitude); Figure 5 shows the global distribution of these stations. From, in total, nineteen sonde launch stations we received 847 profiles. From, in total, eight lidar stations we received 508 profiles. From, in total, four MWR stations we received 849 daily files each containing several profiles.

3.6. GBMCD Data Quality Criteria

[24] Validation of data implies the use of reliable correlative data with known (high) quality for the analysis. Therefore, in this analysis, we have used data from networks with regular calibration and validation activities. In Table 1 we have indicated which contributions come from stations that are part of the Network for the Detection of Stratospheric Change (NDSC). The initiative for this network [*Network for the Detection of Stratospheric Change*, 1986] (http://www.ndsc.ws) was based on the need for such worldwide high-quality measurements, among others for validation of satellite-based sensors. The NDSC comprises a small number of ground-based measurement stations employing the full suite of instruments and located on strategic positions on the globe, and they are supplemented with measurements performed at complementary stations. The measurements of NDSC are regularly monitored for their quality via measurement validation campaigns performed under the NDSC protocol. See, for example, the papers about the STOIC [*Margitan et al.*, 1995], MLO95 [*McPeters et al.*, 1999], OPAL [*McDermid et al.*, 1998a, 1998b], OHP97 (G. O. Braathen et al., manuscript in preparation, 2004) and NAOMI [*Steinbrecht et al.*, 1999] campaigns, at the Table Mountain, Mauna Loa, Lauder, OHP, and Ny-Ålesund NDSC stations, respectively. A review paper of all these activities has recently been composed by *Keckhut et al.* [2004]. Other data contributors that are not NDSC members (note that this only involves sonde data) are generally part of other networks like those stations contributing to the World Ozone and Ultraviolet Radiation Data Center (WOUDC) and the Southern Hemisphere Additional Ozonesondes (SHADOZ) project (see Table 1).

[25] To increase quality further, we have chosen to limit the use of the GBMCD correlative data by taking into account the known strength and weaknesses of the different instruments, which have become clear from the experience obtained in the validation campaigns mentioned above and the intrinsic limitations of the three types of correlative instruments. We restrict the use of correlative data by applying uniform selection criteria, in this way avoiding the need to analyze individual profile quality and necessary range restrictions. The altitude ranges of the three different

Table 1. Overview and Details of Stations and Instruments Providing Correlative Data[a]

Location[b]	Latitude	Longitude	Instrument	Profiles	AO ID	Instrument PI Name	Institute[c]
Ny-Ålesund (P)	78.92	11.93	lidar	115	331	P. von der Gathen	AWI
Ny-Ålesund (P)	78.92	11.93	sonde	74	331	P. von der Gathen	AWI
Thule (P)	76.53	−68.74	sonde	26	158	S. Andersen	DMI
Scoresbysund (C)	70.48	−21.97	sonde	34	158	S. Andersen	DMI
Alomar (C)	69.30	16.00	lidar	54	9079	G. Hansen	NILU
Kiruna (C)	67.84	20.41	microwave	103	191	U. Raffalski	IRF
Sodankylä (C,W)	67.37	26.63	sonde	78	429	E. Kyrö	FMI
Keflavik	64.00	−22.00	sonde	25	191	M. Gil	INTA
Orland	63.40	9.20	sonde	19	158	A. Vik	NILU
Yakutsk (C)	62.02	129.63	sonde	4	158	V. Dorokhov	CAO
Jokioinen (W)	60.81	23.50	sonde	27	429	E. Kyrö	FMI
Legionowo (C)	52.40	20.97	sonde	48	174	B. Kois	IMWM
De Bilt (C,W)	52.10	5.18	sonde	47	174	M. Allaart	KNMI
Uccle (C,W)	50.80	4.35	sonde	114	300	D. De Muer	RMIB
Hohenpeissenberg (C,W)	47.80	11.02	lidar	24	360	H. Claude	DWD
Hohenpeissenberg (C,W)	47.80	11.02	sonde (BM)	32	360	H. Claude	DWD
Payerne (C,W)	46.82	6.95	sonde	113	158	R. Stubi	MeteoSwiss
Payerne (C)	46.82	6.95	microwave	275	158	N. Kaempfer	MeteoSwiss
Observatoire de Haute-Provence (P)	43.94	5.71	lidar	83	360	S. Godin-Beekmann	CNRS
Toronto (C)	43.66	−79.4	lidar	5	153	S. Pal	MSC
L'Aquila	42.34	13.33	sonde	3	206	G. Visconti	UNIVAQ
Table Mountain (C)	34.40	−117.70	lidar	76	360	I. S. McDermid	JPL
Mauna Loa (P)	19.54	−155.58	lidar	87	360	I. S. McDermid	JPL
Mauna Loa (P)	19.54	−155.58	microwave	257	179	A. Parrish	UMass and NIWA
Paramaribo (C,W,S)	5.75	−55.20	sonde	39	174	M. Allaart	KNMI
Lauder (P)	−45.04	169.68	lidar	64	9003	D. Swart	RIVM and NIWA
Lauder (P)	−45.04	169.68	microwave	214	179	A. Parrish	UMass and NIWA
Lauder (P)	−45.04	169.68	sonde	57	179	G. Bodeker	NIWA
Marambio (W)	−64.20	−56.70	sonde	42	429	E. Kyrö	FMI
Dumont d'Urville (P)	−66.67	140.01	sonde	27	158	F. Goutail	CNRS
Belgrano	−78.00	−38.00	sonde	28	191	M. Yela	INTA

[a]The details include the network affiliation, the ESA AO project number, and the principle investigator (PI) of the instrument.
[b]P, Network for the Detection of Stratospheric Change (NDSC) primary station; C, NDSC complementary station; W, World Ozone and Ultraviolet Radiation Data Center (WOUDC) station; S, Southern Hemisphere Additional Ozonesondes (SHADOZ) station; BM, Brewer/Mast ozonesonde type.
[c]AWI, Alfred Wegener Institute for Polar and Marine Research; DMI, Danish Meteorological Institute; NILU, Norwegian Institute for Air Research; IRF, Swedish Institute of Space Physics; FMI, Finnish Meteorological Institute; INTA, Instituto Nacional de Técnica Aeroespacial; CAO, Central Aerological Observatory; IMWM, Institute of Meteorology and Water Management; KNMI, Royal Netherlands Meteorological Institute; RMIB, Royal Meteorological Institute of Belgium; DWD, Deutscher Wetterdienst; CNRS, Centre National de la Recherche Scientifique; MSC, Meteorological Service of Canada; UNIVAQ, University of L'Aquila; JPL, Jet Propulsion Laboratory; UMass, University of Massachusetts; NIWA, National Institute of Water and Atmospheric Research; RIVM, National Institute for Public Health and the Environment.

instruments are restricted to those ranges where known optimal quality and highest altitude resolution prevails. On the basis of this, we have chosen to use sonde data between 0- and 30-km altitude, lidar data between 18- and 45-km altitude, and MWR data between 30- and 70-km altitude. Even though the MWR data has good quality in the 20- to 30-km range, we have chosen to only use lidar and sonde data, because of their higher altitude resolution.

[26] Despite the restricted altitude range for each instrument, it was also necessary to remove parts of the remaining profiles from lidars and MWRs. As some lidars are operated in daytime mode, they have a lower sensitivity because of the higher straylight intensity, and the upper altitude limit of good-quality data is lower than 45 km. In addition, some profiles of the MWRs have a lower quality, which is also related to observational parameters. Therefore the lidar and MWR data are further restricted and only used when their reported relative error is smaller than 30%. The sonde data are reported without an error estimate and therefore we cannot restrict them further in this way. One could argue that the error restriction is sufficient and we do not need to also restrict the altitude range. However, as some errors are reported as rather constant, mainly systematic, errors, this could introduce biases in altitude ranges where the instruments have known limitations, because the smaller ozone values compared to the larger values are more likely to be removed, as they will have a larger relative error.

3.7. Collocation Criteria

[27] All the profiles that are mentioned in section 3.5 and restricted according to section 3.6 are potentially available for comparison to GOMOS ozone profiles. However, these correlative instruments do not exactly sample the same atmosphere as the satellite instrument, and in order to compare them, we need to define criteria that allow a certain (maximum) difference in both location and time between the two observations. Note that allowing a larger time difference will result in a linear increase of the number of collocated measurements, while increasing the allowed radius around an observation will result in a quadratic increase of collocations. In addition, because of the differences between the instruments in measurement technique and geometry, even a perfect collocation of their observations will always leave differences in the sampled air mass and the sampling duration.

[28] In previous studies [*Meijer et al.*, 2003b; *Veiga et al.*, 1995] it has been demonstrated that a 20-hour time window and a circle with an 800-km radius are appropriate choices for the allowed temporal and spatial differences, respectively. The time collocation criterion is set for the altitude levels

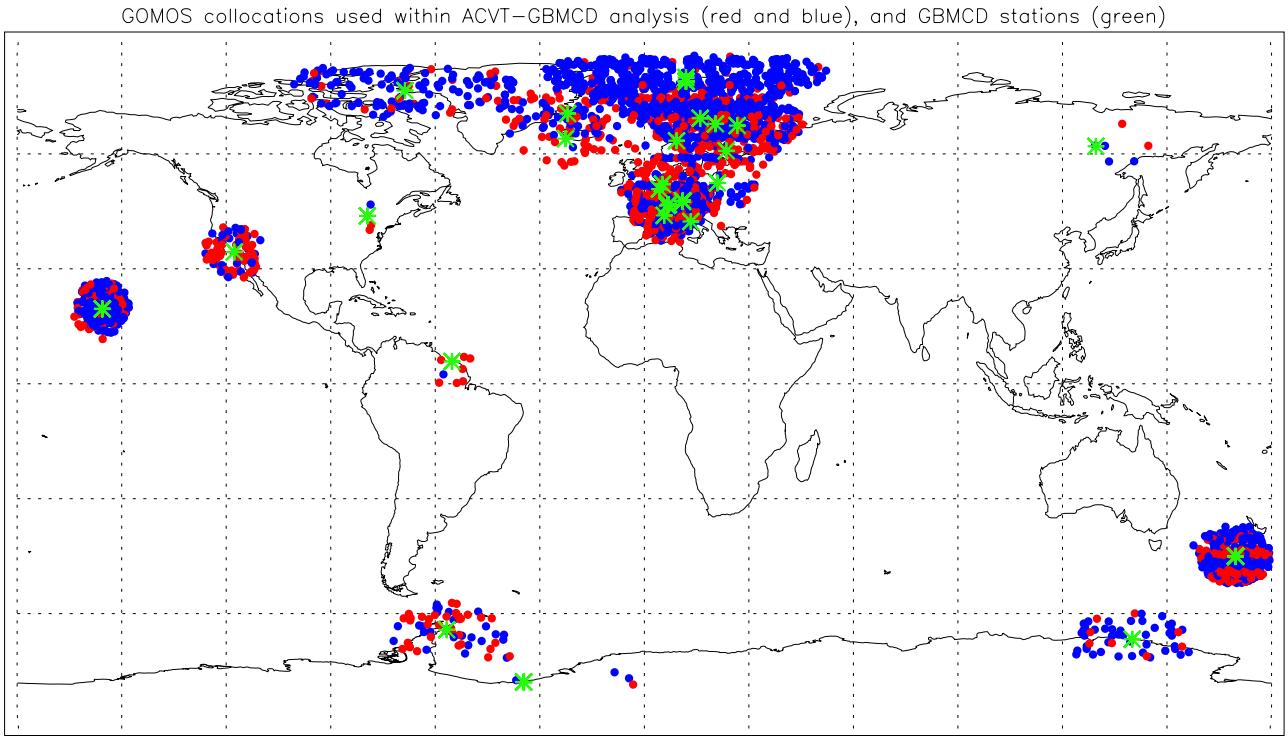

Figure 5. Geolocations of all 3623 available GOMOS measurements collocated (in time and space) with data from the contributing measurement stations (green asterisks). A distinction has been made between measurements made in bright limb (red dots) and twilight or dark limb (blue dots) conditions. Data shown were measured within an 800-km radius and a maximum 20-hour time difference of a GBMCD observation. The sparse availability of GOMOS data around the (tropical) Paramaribo and (Antarctic) Belgrano stations is remarkable and is in contrast to their average data provision (Table 1).

below 50 km. Because in the mesosphere the ozone profile is subject to a strong diurnal variation, we need a stricter time criterion above 50-km altitude, where it is reduced to 5 hours and additionally we require that the profiles were measured under the same limb illumination conditions (defined in section 5). All these criteria form a good compromise between perfect collocations (i.e., sampling exactly the same atmosphere) with insufficient statistics and a large number of poorly collocated observations. Note that because of accurate planning of the sonde and lidar observations, and continuous operation of the MWRs, the collocation criteria relate to maximum differences, and often much smaller differences were achieved. In section 5, we devote section 5.2.7 to investigate the effect on the analysis results of setting different collocation criteria.

[29] The geographical distribution of all 3623 GOMOS measurements used in the analysis is shown in Figure 5. Colors indicate the limb conditions during the measurement. Note that the numbers of collocated GOMOS measurements for the high-latitude stations are larger than those at lower latitudes, which is inherent to Envisat's polar orbit and related measurement density.

4. GOMOS Data Quality Filtering

4.1. Introduction

[30] Initially, our activities had to be focused on excluding from the analysis those (parts of the) GOMOS profiles which have an obvious poor quality, because even before comparing the GOMOS to the GBMCD data it is clear that the data contain some unrealistic features that will hamper the analysis. In Figure 6 we present an example of a normal and an unrealistic GOMOS ozone profile. In addition, we show in this figure the same profiles after using the quality flags provided in the v4.02 data product, but these flags do not seem to have a clear positive effect in the sense of quality filtering. Hence we used the GOMOS data without applying them, but obviously there is a need for a better quality filter. The products of the next released version (v5.0) will contain additional quality flags to allow more effective filtering. A better filter should be easy to implement for future users, and should avoid the need to check each individual profile. We now need to formulate rejection criteria that satisfy this requirement.

4.2. GOMOS Data Quality Criteria

[31] In this paper, we will investigate whether there is a bias present in the GOMOS data. Actually, the investigation of the reported error bars could be the subject of another study. In the analysis presented later in section 5, we will not weigh the mean of the differences with the reported errors, and hence avoiding the mixture of these different investigations. Though, to prevent obviously wrong data entering the analysis, we have only analyzed data with a reasonable error, and then treated them equally. Therefore the following three basic criteria are used for the GOMOS ozone profile data to be accepted in the validation analysis. First, we require an error lower than 20%. This upper limit

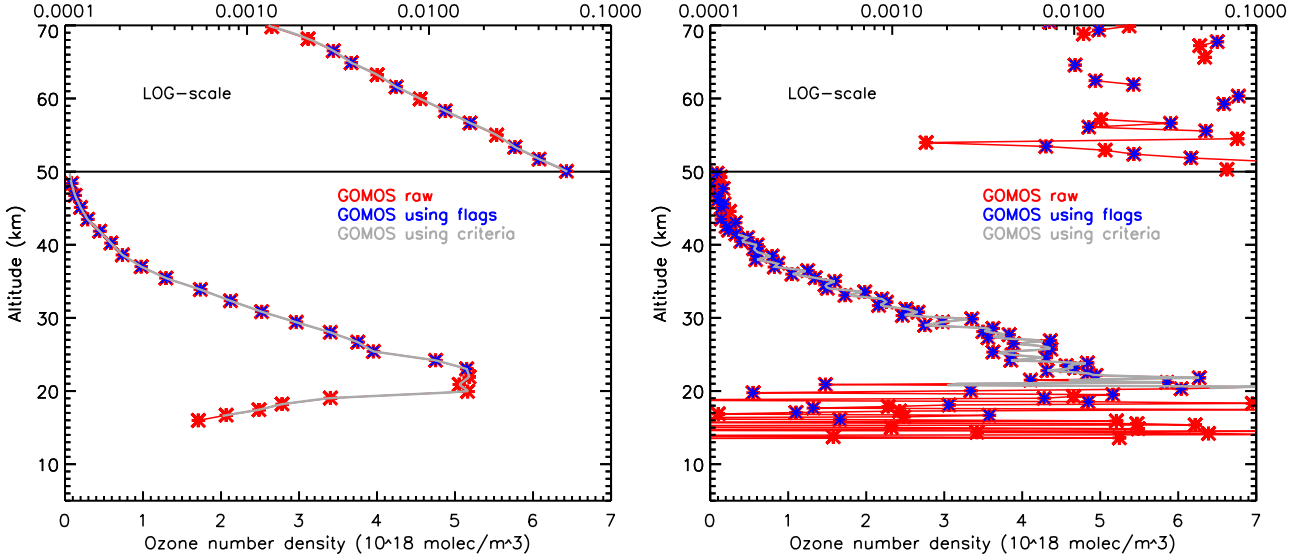

Figure 6. Examples of (left) a realistic GOMOS ozone profile (acquired on 5 September 2002) and (right) a physically unrealistic profile (acquired on 25 November 2002). Both profiles are plotted 3 times: once plotting (all) the original data (lines and asterisks in red), once plotting only those original data accepted according to the quality flags supplied in the data product (blue asterisks), and once plotting only those original data accepted according to the quality criteria set in section 4.2 (gray lines). Note the rather random selection of profile elements at the lowest and highest altitudes using the quality flags, like the rejection of (seemingly) correct elements at the lower altitudes (left panel).

has been set taking into account that the error estimates of v4.02 data are generally too low. Note that v5.0 products will contain significantly improved error estimates, and this criterion may therefore require review when applied to v5.0 products. Nevertheless, we have also checked whether the conclusions drawn from the analysis results would change with an upper limit of 15% and 25%, respectively. However, as the error below (and also above) a certain altitude dramatically increases, such a change in the upper limit only affects a very limited range at the bottom (and top) end of the profile, and has its largest impact on the data measured under bright atmospheric limb conditions. Second, to avoid a possible random selection of data points at the edges, we want the resulting ozone profile to be consistent. Therefore we require that the ozone profile elements accepted so far must also have a significant number of accepted neighboring elements. This second criterion has been implemented by requiring that over a 2-km altitude range around a (candidate) accepted element at least 80% of the original elements should still be present. This consistency check only removes ~2% of the data points and has only a minor impact on the results at the lowest altitudes. Its effect on the analysis has been tested and was mainly visible in the calculated mean and not in the median, which indicates that some outliers that "accidentally" passed the initial criterion are now removed. Third, the remaining profile must at least have a vertical extension of 4 km, because criteria 1 and 2 might result in "profiles" with only a few data points and they will be removed by using this criterion. In Figure 6 we have additionally plotted the profiles resulting from the application of these three criteria to the original GOMOS data.

[32] All GOMOS profiles, which were selected as collocated measurements, are shown in Figure 7 (left panel), which shows both the original profiles (in red), as read from the datafiles without applying the flags, and the accepted profiles (in green) after applying the above-mentioned selection criteria. The actual range of the original data extends up to 10^{21} molecules/m^3, but such a range would reduce the clarity of the plot. The large spread in the main ozone peak stems from the large range in latitude and season covered by these measurements. The effect of the applied quality filtering is clearly visible, but actually this picture gives a wrong impression and is overshadowed by the results of the filtering on the data measured under bright atmospheric limb conditions. The same picture only showing data measured under dark atmospheric limb conditions (right panel of Figure 7) shows that the effect on these data is mainly a rejection of the data at the lowest part of the profile.

4.3. Analysis of Rejected Profile Elements

[33] The use of the quality criteria resulted in an overall rejection of nearly 45% of the original GOMOS data, which certainly makes it worth investigating which parameters cause either acceptance or rejection of a certain altitude level or complete profile. Initially, we focus on the percentage of accepted levels with respect to the number of levels in the original data. We have checked this percentage for dependence on certain GOMOS observational parameters, such as the star magnitude, the star temperature, and/or the solar zenith angle (SZA) during the stellar occultation. The percentage of accepted levels does not have a clear correlation with just one single parameter, but it does show a strong correlation with the star temperature and the SZA, shown in Figure 8. To illustrate the effect of the SZA, we have colored the points corresponding to three different SZA ranges. Although the SZA is an important parameter

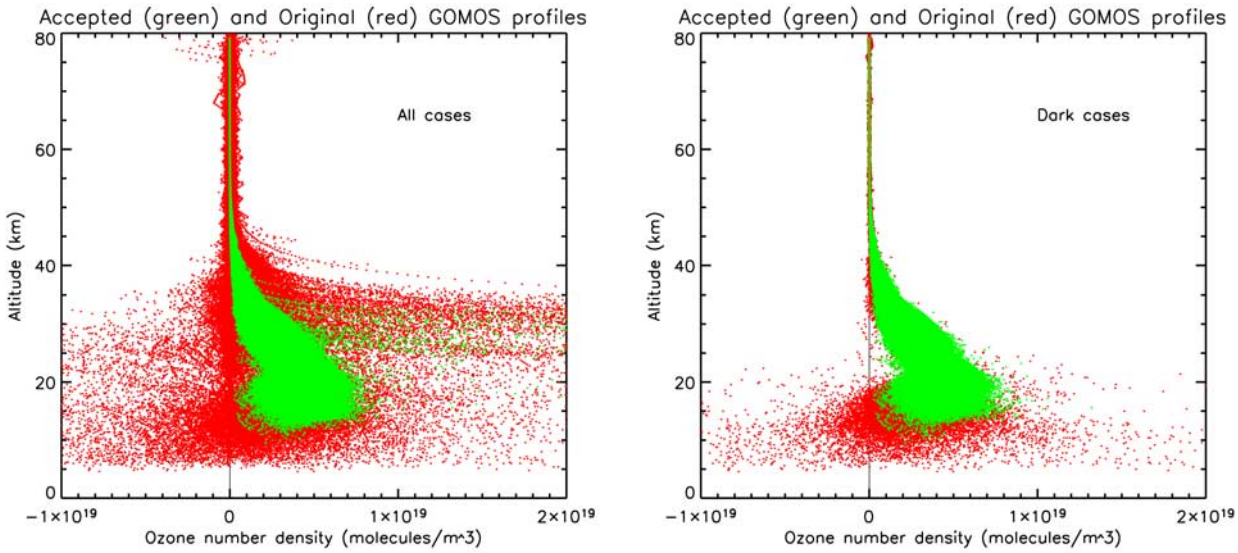

Figure 7. (left) All 3623 GOMOS ozone profiles before (red) and 2845 profiles after (green) applying the quality filter criteria (see Table 3 for statistics). The large range of unrealistic values is clearly visible, which stresses the need for these criteria. (right) Similar to the figure shown in the left panel, but only showing the GOMOS data measured under dark atmospheric limb conditions, which demonstrates that most unrealistic profiles stem from data measured under bright or twilight conditions (see Table 2 for definitions).

for the number of accepted levels, it is also clear from the color indexing that the SZA alone does not give the complete picture. The largest number of accepted levels occurs when the star temperature is high (as expected from the results in Figure 4) and the SZA is large. Note that measurements made with a SZA smaller than 90° correspond to an observation made under bright atmospheric limb conditions. Under dark atmospheric limb conditions, a distinction can be observed between the results measured below and above a star temperature of ~7000 K, and the "average" altitude range covered by the profiles in these regimes are approximately 18–45 and 18–80 km, respectively, which corresponds well with the simulations presented in Figure 4 and the chosen upper limit of the allowed error range. Note that here 80-km altitude is the top of our analysis range. In Figure 8 we additionally observe that the number of accepted levels is generally halved when a star is observed in a bright compared to a dark atmospheric limb.

[34] We have also checked whether a profile has been rejected completely, arising from criterion 3. We have calculated a "star usability," by calculating the number of accepted profiles as a percentage of the total number of available profiles from that star. Figure 9 shows this percentage as a function of star ID number. Note that an identification number (star ID) has been given according to their visual magnitude; i.e., the brightest star has star ID number 1. Stars that have been used less than 5 times in the analysis are colored in gray. We can identify 20 stars (out of 160) that in only 10% (or less) of the measurements lead to an acceptable profile, based on the three selection criteria. This aspect should be further investigated, which can be particularly important for the GOMOS mission planning, as it should be resolved what is the common parameter of these stars and to check their usability on a larger data set, but it is beyond the scope of this paper. From the analysis above, we can conclude that the rejection is correlated to a low star temperature and bright limb conditions, but possibly there are more star characteristics that need to be taken into account. A larger data set spanning a complete year is required to complete this analysis, which should include all stars measured under different conditions. Note that depending on the position of the Earth in the universe,

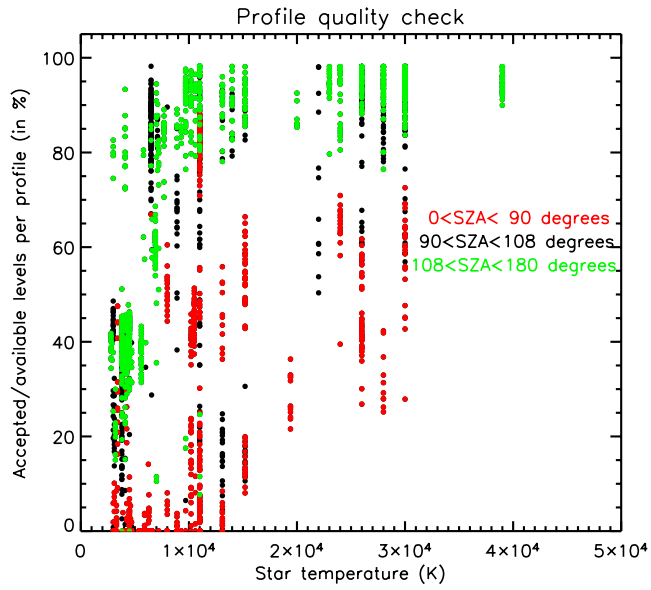

Figure 8. Analysis of profile quality expressed as the percentage of accepted levels as a function of the star temperature. Three different SZA ranges are indicated in color, corresponding to bright (red), twilight (black), and dark (green) atmospheric limb conditions (see Table 2 for definitions).

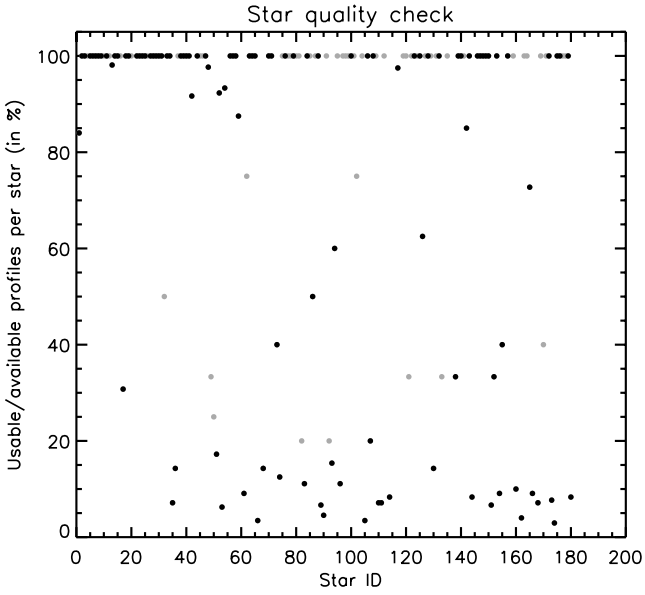

Figure 9. Analysis of star quality expressed as the percentage of usable profiles as a function of the star ID number. Stars that had less than five profiles available for this analysis are in gray. Note the group of stars at the bottom, whose measurements almost always result in a completely rejected profile.

one star can only be observed setting in the atmosphere on either one position or two opposite positions on Earth. Hence using only GOMOS measurements collocated with certain ground-based stations might bias the conclusions of this section on the star quality.

5. Analysis

[35] The aim of this paper is to assess the quality of the GOMOS ozone profiles and possible dependencies on certain parameters. As mentioned in section 2.3, this quality is expected to be dependent on the differences in the brightness and temperature in the large ensemble of targeted stars. Simulations demonstrated (Figure 4) that the quality in the lower stratosphere is expected to be determined by the star magnitude, while at higher altitudes the star's temperature is more important, as hot stars produce significant emission in the UV part of the spectrum. Nevertheless, we should be aware that this expected effect might have been eliminated, because we have selected data (from hot and cold stars) within the same error range, and the errors of the simulations shown in Figure 4 are random and not systematic. In addition, the retrieval seems to be strongly affected by the brightness of the atmosphere in which the star occults. The final observational parameter that we investigate is the inclination of the spatial location of the profile with respect to the vertical. This obliqueness of the occultations depends directly on the LOS angle with respect to the antiflight direction, due to the occultation geometry and the orbital motion. The best results are expected for angles close to zero degrees (i.e., looking backward), because in these "vertical" occultations the scintillation correction for all wavelengths is less complex than in the oblique ones. Apart from these measurement-related parameters, the analysis of profile quality is also performed with respect to the latitude band and the applied collocation criteria. In Table 2 we have listed the parameters and their ranges, which were used in analyzing the comparisons. In section 5.1 we first explain the comparison approach before presenting the analysis results.

5.1. Comparison Approach

[36] The comparison of different data sets raises several important issues about their comparability. The differences in retrieved measurement units have already been accounted for in section 3.2 and 3.4, by transforming all data to values of ozone number density versus geometric altitude. To be able to compare both profile sets, we have linearly interpolated all profiles to a common altitude grid with 200-m intervals.

[37] Between the profiles there can also be differences in the altitude resolution, but taking this into account can become very complicated. For the comparisons involving lidar and sonde data, the effects of ignoring these differences are expected to be small, as these data have quite similar resolutions as those estimated for GOMOS. For the comparisons involving MWR data the situation is different, and the most appropriate way of comparing these data to other data would be to multiply the GOMOS profiles with the MWR averaging kernels and to incorporate their a priori information [*Connor et al.*, 1991]. However, when comparing the data sets in this manner, then the GOMOS data has been degraded and moreover is no longer independent from the MWR data, as shown by *Meijer et al.* [2003b].

Table 2. List of Analysis Parameters Used in the GOMOS Ozone Profile Quality Assessment and Their Applied Ranges

Parameter	Selection 1	Selection 2	Selection 3
Atmospheric limb, deg SZA	0°–90° (bright limb)	90°–108° (twilight limb)[a]	108°–180° (dark limb)[a]
Star visual magnitude M_v	−2 to +1 (strong star)	+1 to +4 (weak star)	–
Star temperature, K	1000–7000 (cold star)[b]	7000–40,000 (hot star)[b]	–
LOS azimuth angle, deg	−10° to +10° (back LOS)	+10° to +45° (slant LOS)	+45° to +90° (side LOS)
Latitude, deg	0°–23.5° (tropical)[c]	23.5°–66.5° (midlatitude)	66.5°–90° (polar)[d]
Collocation criteria (space and time)[e]	0–800 km and 0–20 hours (Δx = 800 and Δt = 20)[e]	0–400 km and 0–10 hours (Δx = 400 and Δt = 10)[e]	0–200 km and 0–5 hours (Δx = 200 and Δt = 5)

[a]Astronomical twilight ends when the Sun is more than 18° below the horizon and the upper atmosphere is no longer illuminated.
[b]The temperature separating the two regimes observed in the (dark limb) results of Figure 8 is taken as the border.
[c]Latitudes of the Tropic of Capricorn (SH) and Cancer (NH) are taken as the border between the tropical and midlatitude regions.
[d]Latitudes of the Antarctic (SH) and Arctic (NH) circles are taken as the border between the midlatitude and polar regions.
[e]Above 50-km altitude the time criterion is always 5 hours.

Table 3. Statistics of GOMOS Collocated Observations Used in This Study

	Statistic	Reduction	Total Left Over
1	GOMOS-GBMCD collocated observations		6747
2	unavailable GOMOS files	−3063	3684
3	corrupt or empty GOMOS files	−61	3623
4	GOMOS profiles rejected because of quality criteria	−778	2845
5	collocated pairs without altitude overlap	−343	2502
	GOMOS-GBMCD pairs used in this study		2502

[38] In this paper, we make the assumption that the effects arising from differences in altitude resolution are also negligible for the comparisons involving MWR data. The effect of ignoring such differences is expected to result in a larger standard deviation of the differences between data set 1 and data set 2, and a smaller standard deviation of the profile for the data set with the coarsest resolution. In the calculated mean differences, a small bias might only show up in regions where the profile demonstrates on average strong curvature. Although the altitude resolutions of the MWR and the GOMOS data are quite different, the effects of ignoring these differences are also expected to be small. This results from assuming that the MWR smoothing error (which includes the effects of resolution and a priori information) is stochastic, and hence its mean error should vanish when considering a sufficiently large ensemble of profiles.

[39] The next step is to check whether the paired profiles of GOMOS and GBMCD data exhibit overlapping altitude ranges. This is especially important for those pairs involving sonde measurements, where the data sometimes only reach up to 18-km altitude. Even worse, sometimes the collocated GOMOS profiles do not have any altitude overlap with the GBMCD correlative data, and hence these pairs were not useful. In Table 3 we list the total number of collocated GOMOS-GBMCD observations (pairs), the number of unavailable GOMOS profiles, the number of corrupt or empty GOMOS files, the number of rejected GOMOS files due to the quality criteria, and the number of pairs without altitude overlap. The largest reduction (over 45%) results from unavailable GOMOS data, which is raw GOMOS data that have been taken but have not yet been processed, and we hope to incorporate this set in future studies. Applying the quality criteria to the GOMOS data has an especially large effect on the altitude extent of the profiles, and as a consequence it reduced the number of useful pairs by 343. In addition, the quality criteria have completely rejected 778 GOMOS profiles and hence equally reduced the number of pairs. In total we are left with the respectable number of 2502 useful profile pairs.

[40] From the useful set of collocated pairs, or any subset of them, we calculate the mean and the standard deviation of the GOMOS and GBMCD ozone profiles. In addition, we calculate the mean, the standard deviation, and the median of their differences; calculated as GOMOS minus GBMCD data in percentage relative to the latter. Per altitude level the availability of valid data pairs is evaluated (i.e., is there overlap in altitude), and from these data points we derive all of the above quantities.

5.2. Results

[41] In Figure 10 we present the analysis results for the whole set of useful collocated pairs. Shown are the mean ozone profiles of both data sets (left), the calculated differences (middle), and a comparison of the standard deviations (right). The discontinuities in the left panel profiles (e.g., at 30-km altitude) originate from the differences in the number of pairs used per altitude level, which are partly due to the GBCMD data restrictions. Note that data from different instruments are not always measured in the same latitudinal range or season, and hence these discontinuities can be understood from geophysics. In between the middle and right panel we have indicated for some of the altitude levels the actual number of profile pairs that have been used in the analysis at that particular level.

[42] Ideally, the profiles of the median and mean differences would be equal and the standard deviation of the differences would be relatively small compared to the standard deviation and the error of the GOMOS and GBMCD profiles. When the distribution of the differences contains outliers, then this would be reflected in a large standard deviation (e.g., around 30-km altitude). Those outliers that are only present on one side of the distribution can be identified by differences observed between the median and the mean, which is basically the case over the whole altitude range (Figure 10).

5.2.1. Influence of Limb Illumination Condition

[43] The main source of the discrepancies is the solar illumination condition of the atmospheric limb. We have distinguished between three atmospheric limb conditions, namely, the bright, twilight, and dark limb situation (Table 2), and made subselections of the analysis involving only these GOMOS data; see Figure 11. The bright limb condition clearly influences the GOMOS data resulting in an 18–33% negative bias and a limited altitude extent (top panels of Figure 11). The subselection of bright limb cases was furthermore subdivided to examine the possible (section 2.3) influence of star magnitude and temperature (Table 2) on the retrieval (not shown). The star magnitude has the strongest influence on the analysis results. Whereas the selection with "strong" stars gives results with a 15–25% negative bias between 35- and 64-km altitude, the selection with "weak" stars ranges from −50% bias at 40 km to −15% at 63-km altitude and has a slightly larger standard deviation of the differences. In bright limb the selection with "cold" stars compared to the selection using "hot" stars gives indeed the expected smaller altitude extent, but its bias in the overlapping range is less negative and even oscillating around zero between 30- and 42-km altitude.

[44] Results dramatically improve when the limb is under twilight conditions with a less negative bias, now 12% in the overlapping altitude range and even 5% below 35 km, and with profiles extending down to 12 km (middle panels of Figure 11). Despite the improvements, we observe that above 57-km altitude the twilight limb selection shows an increasing strong positive bias, and the variation of the

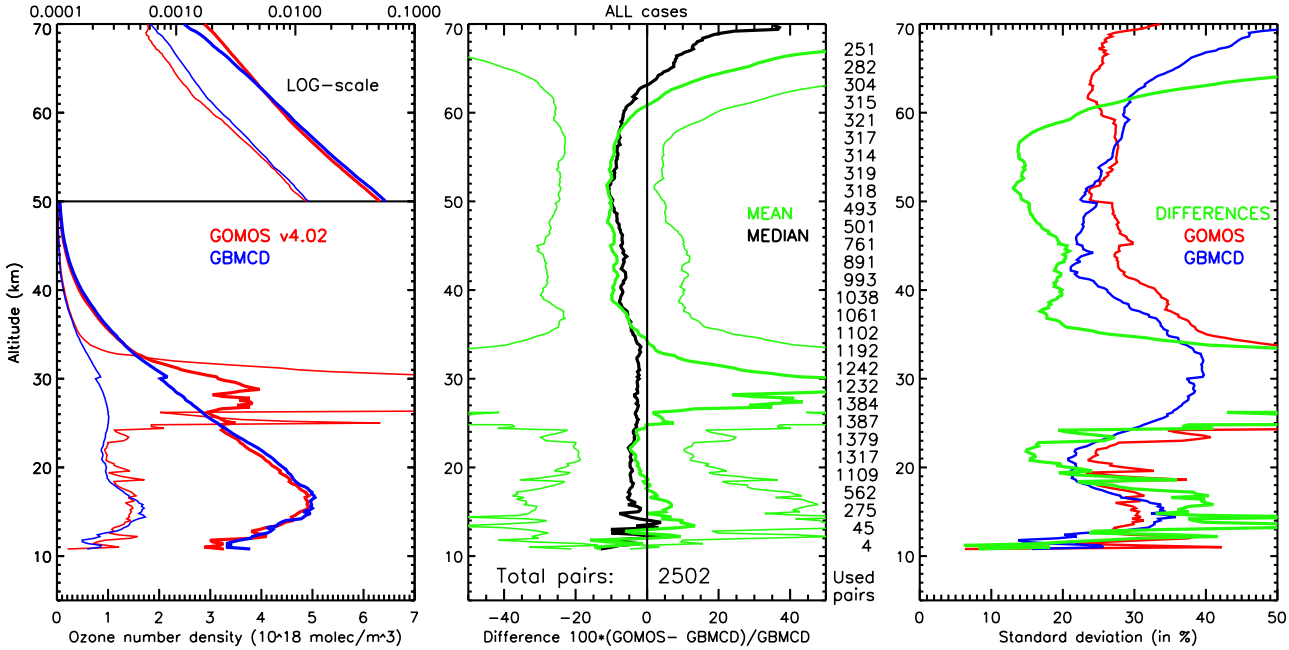

Figure 10. Intercomparison results of all accepted GOMOS and paired GBMCD correlative data. (left) Mean GOMOS (bold red line) and GBMCD (bold blue line) ozone profiles and their standard deviations (thin lines in corresponding colors). Note the logarithmic, instead of linear, scale for the ozone values above 50-km altitude. (middle) Mean (bold green line) and median (black line) differences between all the paired GOMOS and GBMCD data as a percentage of the latter. For the mean profile, we also plotted the (1σ) standard deviation of the differences (thin green line). Numbers at the right of the middle panel indicate, for some altitude levels, the number of pairs used at that level. (right) A comparison between the standard deviation of the differences (green line) and the standard deviation of all GOMOS (red line) and GBMCD (blue line) ozone profiles.

GOMOS ozone profile deviates from the one of the GBMCD over almost the entire altitude range. Note that in this range the time criterion for collocation is 5 hours and that the GBMCD data have also been measured under twilight atmospheric limb conditions.

[45] These poor-quality GOMOS data, in which there might be some solar illumination in the observations (i.e., bright and twilight limb cases), are then removed from the whole selection and this results in the dark limb selection (Table 2). This selection (bottom panels of Figure 11) again improves over those cases measured in twilight limb with a smaller negative bias (especially between 35- and 52-km altitude) and a smaller standard deviation of the differences. From 14- to 64-km altitude the analysis results of this dark limb selection show a small 2.5% negative bias below 45 km that grows slightly to a 7.5% negative bias above this altitude. The standard deviation of the differences decreases from 16% (19–30 km) to 14% (30–45 km) to 11% (45–61 km) with increasing altitude, and is always smaller than the standard deviation (variation) of the GOMOS and GBMCD ozone profiles. Note that the variation in the GOMOS and GBMCD profile pairs is, more or less, equal over the whole altitude range, which adds to the confidence in the quality of the GOMOS data. In addition, between 21- and 62-km altitude the median and mean of the differences are as good as equal, which indicates an even distribution of the analysis results around the mean value.

[46] We conclude that the GOMOS measurements made in dark limb give the best results. Therefore only these dark limb cases (1,376 profiles) will be further analyzed in sections 5.2.2–5.2.7, to check for possible other influences on the GOMOS data quality.

5.2.2. Influence of Star Magnitude

[47] Here we examine the influence of the star magnitude on the analysis results. As there are not so many strong stars, the subselection of the dark limb cases only involves 109 profile pairs versus 1267 pairs with weak stars (top panels of Figure 12). Since the number of pairs is lower, the standard deviation of the differences is expected to be larger, but instead it is even smaller (e.g., above 30 km ~8% instead of ~12%) indicating higher-quality (less noisy) GOMOS profiles for the strong star observations, which results from the (expected) higher-quality spectra. The derived bias for the strong stars is slightly larger below 45 km (−4% versus −2.5%) and slightly smaller above this altitude (−5% versus −7.5%), and the results extend 3 km lower down in altitude. We conclude that there is no significant influence of the star magnitude on the GOMOS data quality.

5.2.3. Influence of Star Temperature

[48] The selections of hot (822 pairs) and cold stars (554 pairs) give almost equal analysis results with only a few small differences (see bottom panels of Figure 12). In general the bias is similar, except between 37- and 54-km altitude where the cold stars show a smaller bias. In

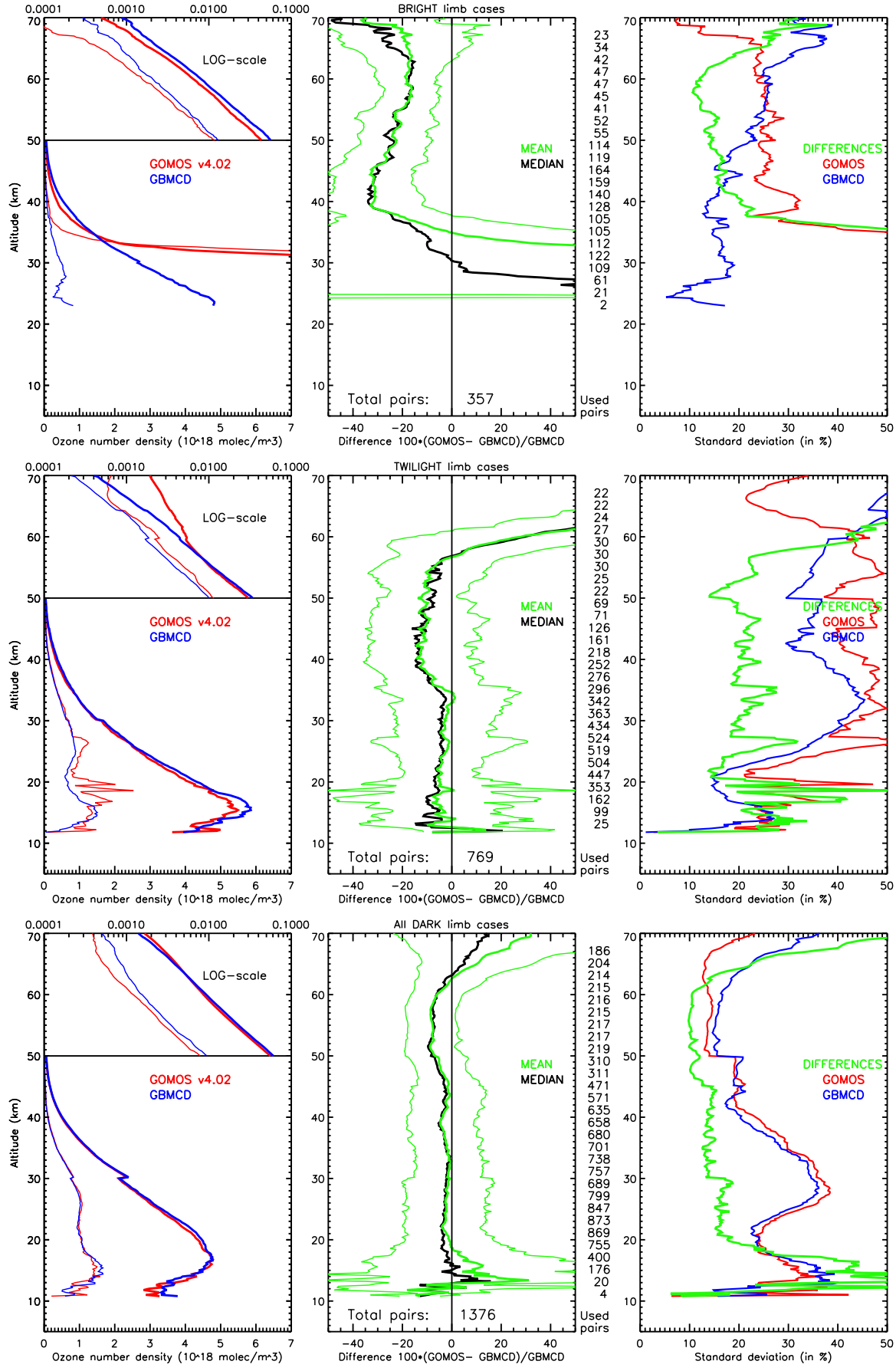

Figure 11

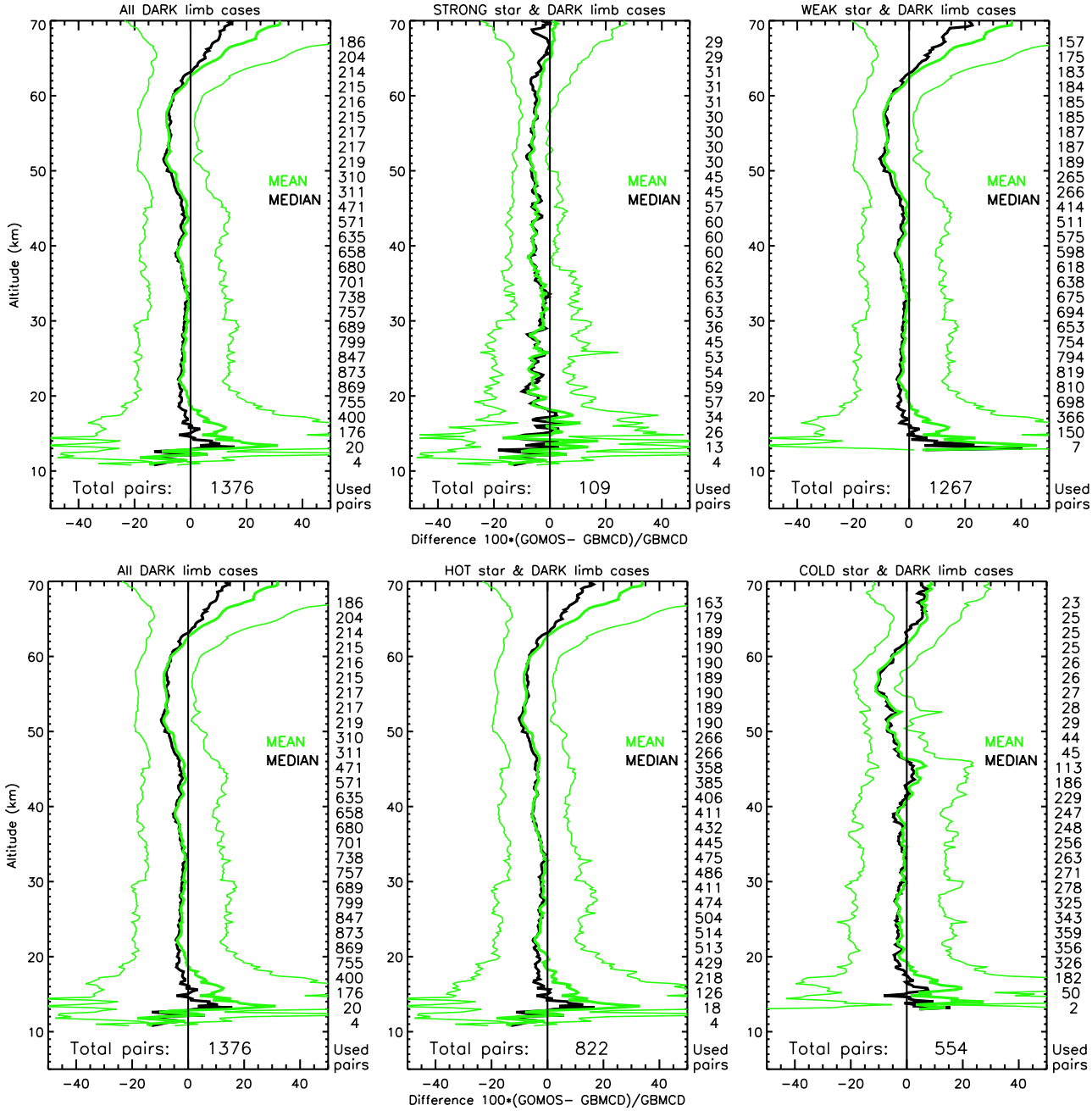

Figure 12. All panels show analysis results similar to those shown in the middle panel of Figure 10. The top panels show the influence of the star magnitude, and these selections only involve those paired data in which GOMOS measured under dark limb conditions and used (top left) all, (top middle) strong, and (top right) weak stars (see Table 2 for definitions). The bottom panels show the influence of the star temperature, and these selections only involve those paired data in which GOMOS measured under dark limb conditions and used (bottom left) all, (bottom middle) hot, and (bottom right) cold stars (see Table 2 for definitions).

addition, the cold stars have a slightly larger standard deviation of the differences at low altitudes and smaller at higher altitudes. The hot stars give results that extend 3 km lower down in altitude, but the overall valid range is the same. We point out that the number of pairs is limited at higher altitudes, just like in the bright limb subselection, which was expected (section 2.3) from simulations and also shown in the analysis of rejected profile elements

Figure 11. Similar to Figure 10, but now using only the subselection of the paired data in which GOMOS measured under (top) bright, (middle) twilight, and (bottom) dark limb conditions (see Table 2 for definitions). Note the differences in total number of pairs.

(section 4.3). Apart from the altitude extent, we conclude that there is no significant influence of the star temperature on the GOMOS data quality.

5.2.4. Influence of LOS Azimuth Angle

[49] In November 2002 the GOMOS instrument encountered a problem with the steering mirror control unit which limited its range over which a star could be viewed setting in the atmosphere. Instead of the nominal −10 to 90 degrees LOS azimuth angle with respect to the antiflight direction, the LOS could only be pointed (initially) from 0 to 90 and later from 4 to 90 degrees. Although the problem has been solved in July 2003 by switching to the redundant mirror control unit, it is worth investigating the possible effect of the LOS azimuth angle on the measurement quality, especially for this period, but also during nominal operations. The analysis results (not shown) of the ''back LOS'' and the ''slant LOS'' selections (see Table 2) are mutually almost identical and very similar to the results of the all dark selection, which is not surprising as it comprises 88% of the pairs. For larger positive LOS azimuth angles (i.e., ''side LOS'' selection, Table 2) the GOMOS data tend to get noisier. Even though the mean bias remains quite similar to the other two selections, this noise results in an increasing standard deviation of the differences, especially toward lower altitudes.

5.2.5. Influence of Geolocation

[50] The previous sections mainly focused on the influence of observational parameters, but in this section we focus on the validity of the GOMOS data in different global regions, which are divided in different latitudinal ranges (Table 2). The comparison results for the polar regions (top panels of Figure 13) show quite large standard deviations of the profiles and of their differences (top right panel). In addition, generally the bias in these regions is slightly more negative than the bias of the whole selection (bottom panels of Figure 11), and especially between 35- and 45-km altitude where the bias is −12%. Above 50 km there are only three pairs left, and above 58-km altitude they show an increasing positive bias.

[51] The midlatitude regions, compared to the polar regions, show much smaller standard deviations. The effect of averaging only data from similar regions is clearly visible in the variation of the ozone profiles, which becomes even more apparent in the tropical regions. In the midlatitude regions (middle panels of Figure 13) there is no bias between 28- and 38-km altitude, and below and above these altitudes there is a slightly negative bias, but within the standard deviation of the differences.

[52] The results for the tropical regions (bottom panels of Figure 13) show a little bit more structure in the profile of mean differences, but the bias is again small. In these regions though, the variation of the profiles is so small that it is even smaller than the standard deviation of the differences. Because of the lack of available GOMOS data collocated with the Paramaribo station, these analysis results contain almost exclusively paired data from the Mauna Loa observatory on Hawaii, United States.

5.2.6. Influence of Correlative Instrument

[53] In order to exclude possible effects introduced by using a specific type of correlative instrument, we have separately analyzed the paired data only involving sonde, lidar and MWR data (the left, middle and right top panels, respectively, of Figure 14). The results are remarkably consistent and the derived bias involving the data of different instruments overlap in the altitude regions in common. Toward the top and bottom end of the allowed lidar altitude range the standard deviation of the differences increases and the mean starts to deviate from the median. The same applies to the top end of the sonde altitude range. From this we conclude that we have made a good choice for the applied GBMCD quality criteria (section 3.6).

5.2.7. Influence of Collocation Criteria

[54] The applied collocation criteria (section 3.7) were assumed to be strict enough to distinguish between dynamically induced differences and any possible biases present in the GOMOS data. Temporal and spatial differences between two observations can, to a certain extent, be regarded as interchangeable variables, because in time atmospheric dynamics moves the air away from a measurement site. Therefore we have investigated the influence of setting stricter criteria by simultaneously tightening both criteria. The selection with all dark limb cases corresponds to the standard 800-km radius and 20-hour time window criteria (bottom left panel of Figure 14). The results for setting 2 times ($\Delta x = 400$ and $\Delta t = 10$) and 4 times ($\Delta x = 200$ and $\Delta t = 5$) stricter collocation criteria are shown in the middle and right bottom panels, respectively, of Figure 14. Note that in all selections the time criterion above 50-km altitude is always 5 hours. It is reassuring to see that the analysis results are very similar for all three selections, and the main difference between them is a slightly decreasing standard deviation of the differences and a noisier mean bias profile. Note that the number of pairs decreases as expected (section 3.7) by a factor of 8 in each step, which would significantly limit the possibility to make further subselections when these stricter criteria would be used. From this we conclude that the chosen criteria for this paper (see Table 2) were appropriate and that there is no need to tighten them.

6. Discussion and Conclusions

[55] The GBMCD subgroup of ESA's ACVT, which is part of Envisat's coordinated validation program, aimed in this paper to assess the quality of GOMOS ozone profiles. This assessment is based on a large number of correlative measurements worldwide and should support the atmospheric research community in the use of these data. We have presented the validation results from GOMOS data generated with the prototype processor version 5.4b, equivalent to v4.02 of the operational processor, and measured between 1 July 2002 and 1 April 2003, which completely includes Envisat's Commissioning Phase. A constituted data set between ground level and 70-km altitude formed the high-quality reference set, which included GBMCD correlative measurements from thirty-one instruments/launch sites at twenty-five stations ranging from the Arctic to the Antarctic. These GBMCD data were successfully used to analyze the GOMOS ozone profile quality, and in addition to investigate several possible dependencies on measurement and geophysical parameters.

[56] Initially, our activities had to be focused on excluding from the analysis those (parts of the) GOMOS profiles that have obvious poor quality, because even before comparing them, it is clear that the data contain some unrealistic

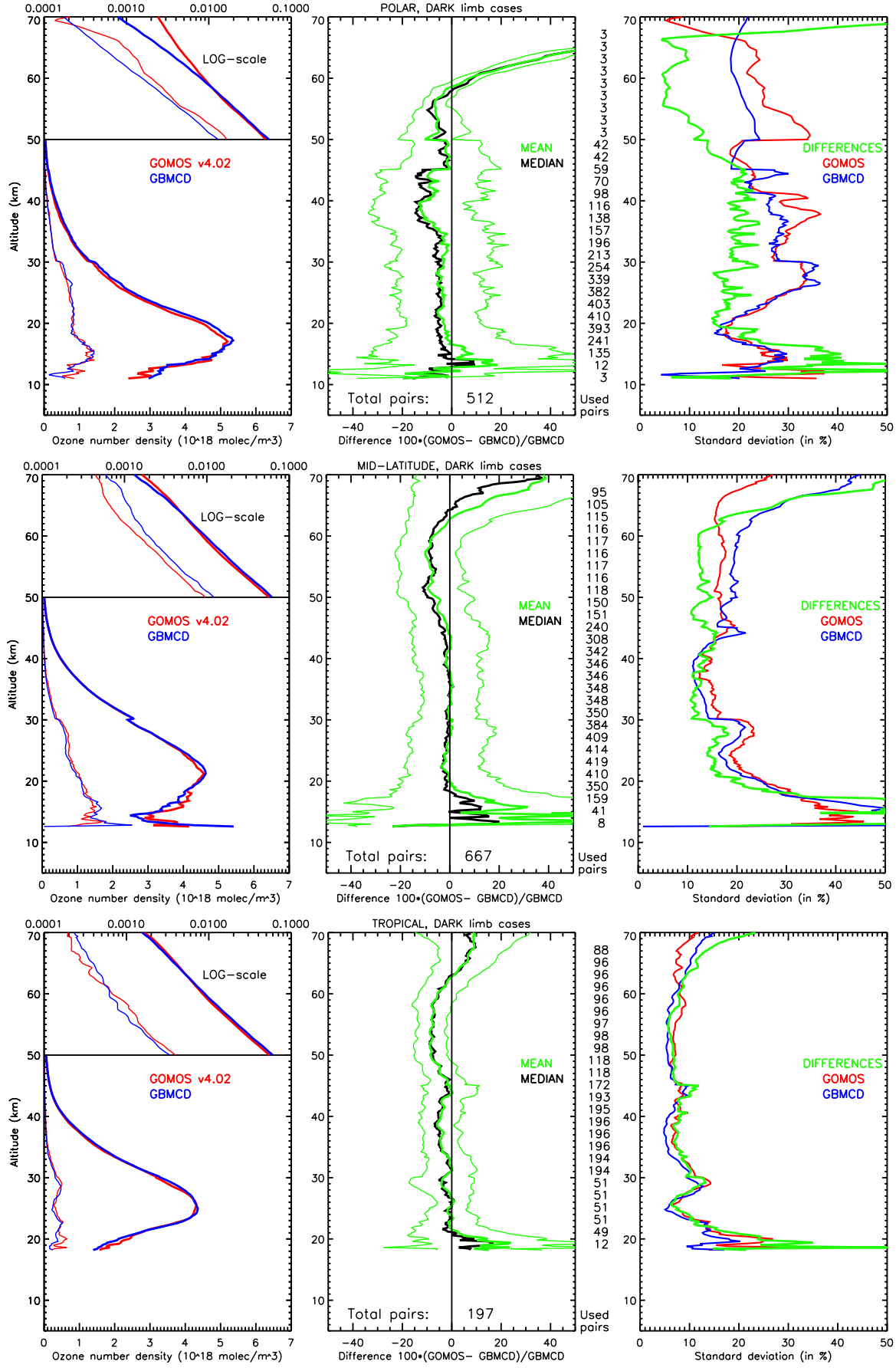

Figure 13

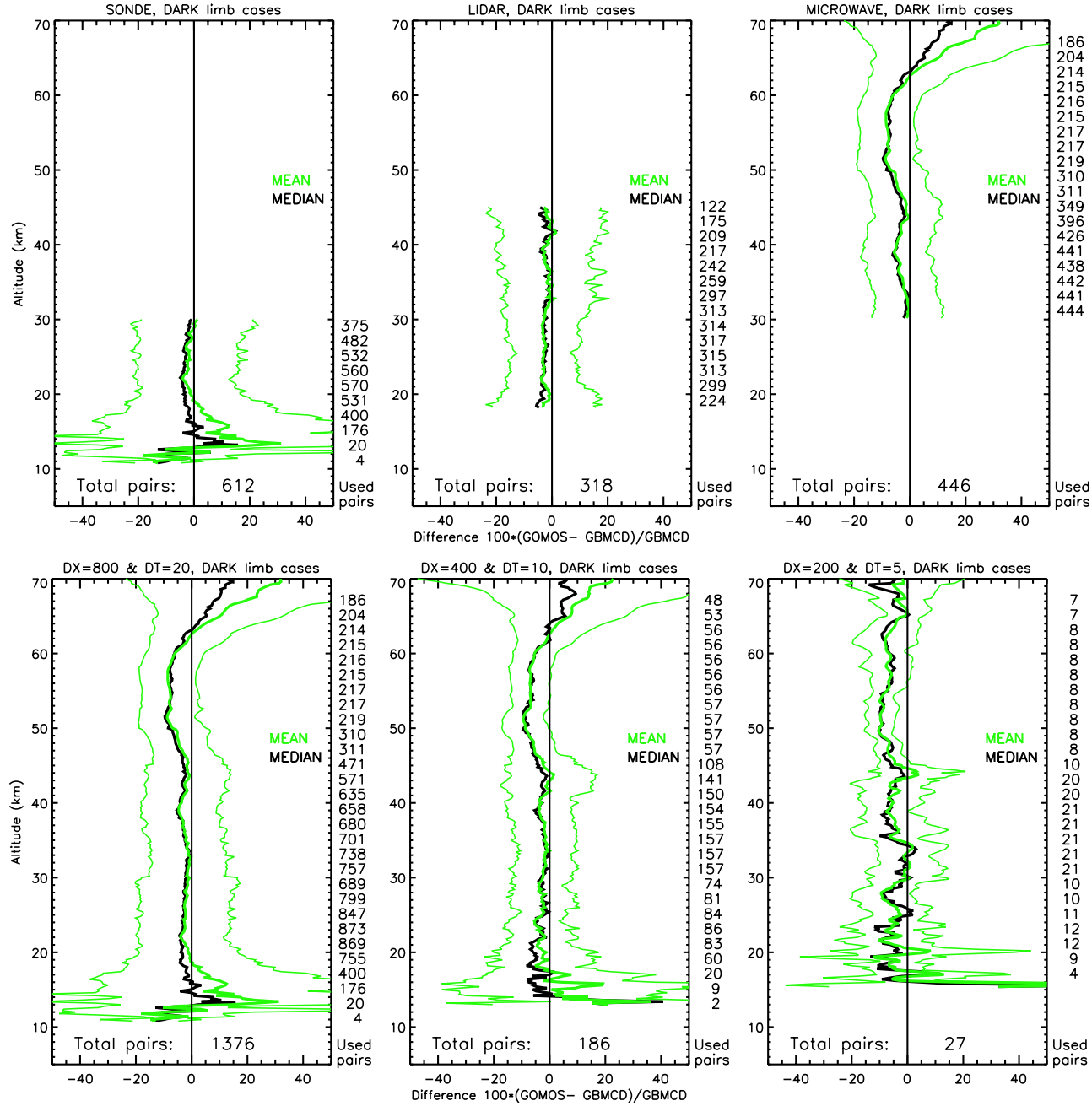

Figure 14. All panels show analysis results similar to those shown in the middle panel of Figure 10. The top panels show the influence of the used correlative instrument, and these selections only involve those data in which GOMOS measured under dark limb conditions and that are paired with (top left) sonde, (top middle) lidar, and (top right) microwave data. The bottom panels show the influence of the applied collocation criteria, and these selections only involve those data in which GOMOS measured under dark limb conditions and that are paired using (bottom left) normal, (bottom middle) 2 times stricter, and (bottom right) 4 times stricter collocation criteria in both space and time (see Table 2 for definitions). Note that the bottom left panel is identical to the "all dark limb" selection (bottom of Figure 11).

features that will hamper the analysis. Therefore we have only selected data with a reasonable error, and we have additionally required that the resulting ozone profile be consistent, which avoids a possible random selection of data points at the edges. Applying these criteria reduced the GOMOS data quantity by nearly 45%, and in 22% of the cases even rejected the whole profile. We found that rejection or acceptance of data is correlated with a combi-

Figure 13. Similar to Figure 10, but now using only the subselection of the paired data measured in the (top) polar, (middle) the midlatitude, and (bottom) the tropical regions (see Table 2 for definitions).

nation of both the star temperature and the atmospheric limb condition. Measurements on hot stars in a dark limb gave the highest number of accepted profile elements. Separating the above-mentioned numbers by atmospheric limb condition gives 77%, 34% and 28% of data quantity reduction, and 55%, 5% and 0.4% of rejected profiles for bright, twilight and dark limb, respectively.

[57] The subset of the original GOMOS data that passed the quality criteria has been validated using lidar, balloon sonde and MWR measurements around the world. In total, we had 2502 available and useful profile pairs, in which correlative observations were performed within an 800-km radius and a maximum 20-hour time difference of a satellite observation. The quality of the GOMOS ozone profiles was found to be strongly dependent on the solar illumination of the limb during the stellar occultation. Data measured under bright limb conditions (i.e., Sun above horizon) give a strong negative bias and their usability is doubtful. Although measurements in twilight limb dramatically improve over those measured in bright limb with a less negative bias, the GOMOS profiles above 57-km altitude show an increasing strong positive bias and over almost the entire altitude range the variation of the profiles deviates from the one of the GBMCD. In the dark limb selection the median and the mean of the GOMOS and GBMCD differences are almost identical between 21- and 62-km altitude with a small (2.5%) negative bias between 14 and 45 km which slightly grows to a 7.5% negative bias above this altitude and up to 64 km. The standard deviation of these differences decreases from 16% (19–30 km) to 14% (30–45 km) to 11% (45–61 km), and in this range is always smaller than the standard deviation (variation) of the GOMOS and GBMCD ozone profiles.

[58] The 1376 profile pairs in which GOMOS measured in dark limb have been used as the basis selection for the remainder of the paper. First of all, the influence of the star characteristics has been investigated. For all the stars used in this intercomparison, both the star apparent magnitude and effective temperature do not seem to have a significant influence on the validation results, but merely on the altitude extent and standard deviation of the differences, which is as expected from simulations. The LOS azimuth angle, at which the star was observed, seems to affect the measurements for angles larger than 45 degrees and in this situation the data is correlated with noise-like features on the ozone profile. Actually, the profile shown as an example in the right panel of Figure 6 has a corresponding LOS azimuth angle of 71 degrees, and demonstrates such an oscillating effect.

[59] Besides the observation-related parameters, we have also analyzed the results for possible dependencies on several geophysical parameters. For example, the analysis has been separated in three different latitude regions. In the polar regions, especially between 35- and 45-km altitude, we found a slightly more negative bias than elsewhere, but note that in these regions for the profile above 50-km altitude there were not enough pairs to draw firm conclusions. In the midlatitude and tropical regions the bias and standard deviation of the differences are small, and between 28- and 38-km altitude at midlatitudes there is even a zero bias. The larger standard deviation of the ozone profiles in the polar regions is expected from the larger seasonal variation of the ozone profile and the increased dynamics compared to the other regions, and this is also reflected in the larger standard deviation of the differences. The increased bias, on the other hand, cannot be explained in this way, unless the increased dynamics or (isotropic) turbulence (e.g., from the vortex) induce errors in the way refraction is described in the retrieval model, but then again this is usually not expected to lead to systematic errors.

[60] On the basis of the above-presented analysis results we have the following recommendations for the users of GOMOS ozone profile data. Provided that the presented quality criteria are applied to the profiles, we believe that it is justified to use the GOMOS data measured under dark limb conditions, which is valid for the altitude range 14–64 km. In this subselection of the GOMOS data the users do not have to consider possible effects of star characteristics and latitudinal region of the measurement, with the exception that in polar regions between 35- and 45-km altitude the bias is slightly larger. They only have to pay attention to possible effects of data measured with a LOS azimuth angle larger than 45 degrees and the inconclusive results above 50-km altitude in the polar regions. Although, the SZA (i.e., limb condition) and the LOS azimuth angle are currently not in the product, they can be supplied by ACRI on request and they will be implemented in the data format with the next processor upgrade.

[61] Future algorithm development should focus on improving the retrieval of data measured in a bright or twilight atmospheric limb and the quality flags in the data product. The quality criteria proposed and applied in this paper indicated that for some specific stars only less than 10% of their occultations yielded an acceptable profile. We recommend further investigation of this aspect and perhaps remove such stars from the measurement list, i.e., priority should be given to other and preferably hot stars. Note that the data examined in this paper did not necessarily enclose all stars observed during the GOMOS mission, which is a consequence of the measurement configuration and the GBMCD geolocations. In addition, we recommend ESA to investigate the (unrealistic) oscillations in the ozone profiles resulting from measurements made with a LOS azimuth angle larger than 45 degrees.

[62] The following conclusions are especially of interest for those researchers who perform validation studies, because in the analysis we have also checked whether the used validation approach influenced the analysis results. First of all, the individual results of the three different instrument types agreed very well, which underlined the quality of the ground-based data set and the validity of the chosen GBMCD data quality criteria. Second of all, when we tightened the allowed spatial and temporal differences between the two observations, the conclusions did not significantly change, and the main difference over the whole altitude range is a smaller standard deviation of the differences (especially below 20-km altitude). This conclusion is also valid for when we apply the same analysis only to data measured in the polar regions. Therefore the chosen collocation criteria (i.e., 800-km radius and 20-hour time window (5 hours above 50-km altitude)) were and are a good compromise between a useful number of collocations and an acceptable similarity of the compared air masses. The above-presented analysis results were uniform up to 61-km

altitude, but above this altitude the results of the different MWRs are diverse and hence inconclusive. In this upper altitude range the averaging kernel and a priori information should be considered in the quality selection criteria of the MWR data, as some instruments and measurement conditions result in poor-quality ozone profiles. Investigating data quality above 61-km altitude should be the focus of future work.

[63] **Acknowledgments.** We greatly appreciate the support and feedback given by the GOMOS quality working group (consisting of ACRI, the Belgian Institute for Space Aeronomy (BIRA), the Finnish Meteorological Institute (FMI), and Service d'Aeronomie du CNRS) and particularly the prompt feedback from the people at ACRI responsible for the GOMOS data processing using ESA's prototype processor. This research was partly funded by a grant from the User Support Program managed by the Program Bureau of External Research of the Space Research Organization Netherlands (PB-SRON). Most of the data used in this publication were obtained as part of the Network for the Detection of Stratospheric Change (NDSC) and are publicly available (see http://www.ndsc.ws). The authors would like to thank ESA and the NILU Cal/Val team for providing data through the Envisat Cal/Val database. The standard data format greatly enhances the accessibility for this kind of large-scale validation activity incorporating multiple data sets. In addition, we would like to acknowledge the tremendous effort of our co-workers involved in measuring, processing, and uploading all the correlative measurements. We are grateful to the following agencies and institutes for their financial support to part of the GBMCD measurements used in this study: ASI (Italy), CNES (France), CSA (Canada), DMI (Denmark), ESA, European Union, Federaal Wetenschapsbeleid (Belgium), INSU (France), IPEV (France), MeteoSwiss (Switzerland), MSC (Canada), NASA, NIVR (Netherlands), NIWA (New Zealand), and SNF (Denmark).

References

Bertaux, J. L., G. Megie, T. Widemann, E. Chassefiere, R. Pellinen, E. Kyrölä, S. Korpela, and P. Simon (1991), Monitoring of ozone trend by stellar occultations: The GOMOS instrument, *Adv. Space Res.*, *11*(3), 237–242.

Bertaux, J. L., et al. (2004), First results on GOMOS/Envisat, *Adv. Space Res.*, *33*, 1029–1035.

Bhartia, P. K., R. D. McPeters, C. L. Mateer, L. E. Flynn, and C. Wellemeyer (1996), Algorithm for the estimation of vertical ozone profiles from the backscattered ultraviolet technique, *J. Geophys. Res.*, *101*, 18,793–18,806.

Connor, B. J., A. Parrish, and J.-J. Tsou (1991), Detection of stratospheric ozone trends by ground-based microwave observations, *Proc. SPIE Int. Soc. Opt. Eng.*, *1491*, 218–230.

Dalaudier, F., V. Kan, and A. S. Gurvich (2001), Chromatic refraction with global ozone monitoring by occultation of stars: I. Description and scintillation correction, *Appl. Opt.*, *40*(6), 866–877.

DeMajistre, R., and J.-H. Yee (2002), Atmospheric remote sensing using a combined extinctive and refractive stellar occultation technique: 2. Inversion method for extinction measurements, *J. Geophys. Res.*, *107*(D15), 4260, doi:10.1029/2001JD000795.

European Space Agency (ESA) (2002), *Envisat GOMOS Product Handbook, Issue 1.1*, ESA Publ. Div., Dec.

European Space Agency (ESA) (2003), Proceedings of Envisat Validation Workshop (Frascati, Italy, 9–12 December 2002), *Eur. Space Agency Spec. Publ.*, *ESA SP-531*.

Kan, V., F. Dalaudier, and A. S. Gurvich (2001), Chromatic refraction with global ozone monitoring by occultation of stars: II. Statistical properties of scintillations, *Appl. Opt.*, *40*(6), 878–889.

Keckhut, P., et al. (2004), Review of ozone and temperature lidar validations performed within the framework of the Network for the Detection of Stratospheric Change, *J. Environ. Monit.*, *6*, 721–733.

Komhyr, W. D. (1969), Electrochemical concentration cells for gas analysis, *Ann. Geophys.*, *25*, 203–210.

Komhyr, W. D., and T. B. Harris (1971), Development of an ECC ozonesonde, *NOAA Tech. Rep. ERL 200-APCL 18*, 54 pp., Atmos. Phys. Chem. Lab., Boulder, Colo.

Kyrölä, E., E. Sihvola, M. Tikka, Y. Kotivuori, T. Tuomi, and H. Haario (1993), Inverse theory for occultation measurements: 1. Spectral inversion, *J. Geophys. Res.*, *98*, 7367–7381.

Kyrölä, E., et al. (2004), GOMOS on Envisat: An overview, *Adv. Space Res.*, *33*, 1020–1028.

Margitan, J. J., et al. (1995), Stratospheric Ozone Intercomparison Campaign (STOIC) 1989: Overview, *J. Geophys. Res.*, *100*, 9193–9208.

McCormick, M. P., J. M. Zawodny, R. E. Veiga, J. C. Larsen, and P. H. Wang (1989), An overview of SAGE I and SAGE II ozone measurements, *Planet. Space Sci.*, *37*, 1567–1586.

McDermid, I. S., S. M. Godin, and T. D. Walsh (1990), Lidar measurements of stratospheric ozone and intercomparisons and validation, *Appl. Opt.*, *29*(33), 4914–4923.

McDermid, I. S., et al. (1998a), OPAL: Network for the Detection of Stratospheric Change Ozone Profiler Assessment at Lauder, New Zealand: I. Blind intercomparisons, *J. Geophys. Res.*, *103*, 28,683–28,692.

McDermid, I. S., et al. (1998b), OPAL: Network for the Detection of Stratospheric Change Ozone Profiler Assessment at Lauder, New Zealand: II. Intercomparison of revised results, *J. Geophys. Res.*, *103*, 28,693–28,699.

McPeters, R. D., et al. (1999), Results from the 1995 Stratospheric Ozone Profile Intercomparison at Mauna Loa, *J. Geophys. Res.*, *104*, 30,505–30,514.

Measures, R. M. (1984), *Laser Remote Sensing*, John Wiley, Hoboken, N. J.

Meijer, Y. J., T. Blumenstock, P. Keckhut, R. Koopman, E. Kyrö, J.-C. Lambert, A. Matthews, S. Pal, H. Schets, and D. Swart (2003a), Analysis of GOMOS ozone profiles compared to GBMCD datasets (bright/dark, star magnitude, star temperature), in *Proceedings of Envisat Validation Workshop (Frascati, Italy, 9–12 December 2002)* [CD-ROM], *Eur. Space Agency Spec. Publ.*, *ESA SP-531*.

Meijer, Y. J., R. J. van der A, R. F. van Oss, D. P. J. Swart, H. M. Kelder, and P. V. Johnston (2003b), Global Ozone Monitoring Experiment ozone profile characterization using interpretation tools and lidar measurements for intercomparison, *J. Geophys. Res.*, *108*(D23), 4723, doi:10.1029/2003JD003498.

Nett, H., J. Frerick, T. Paulsen, and G. Levrini (2001), The atmospheric instruments and their applications: GOMOS, MIPAS and SCIAMACHY, *ESA Bull.*, *106*, 77–87.

Network for the Detection of Stratospheric Change (1986), Report of the workshop in Boulder, Colorado, March 5–7, 1986, Upper Atmos. Res. Program, NASA, Washington, D. C.

Parrish, A., B. J. Connor, J. J. Tsou, I. S. McDermid, and W. P. Chu (1992), Ground-based microwave monitoring of stratospheric ozone, *J. Geophys. Res.*, *97*, 2541–2546.

Ratier, G., G. Levrini, A. Popescu, T. Paulsen, C. Readings, and J. Langen (1999), GOMOS: Envisat's contribution to measuring long-term trends in ozone and other trace gases, *ESA Bull.*, *97*, 8 pp.

Rodgers, C. D. (2000), *Inverse Methods for Atmospheric Sounding: Theory and Practice*, *Ser. Atmos. Oceanic Planet. Phys.*, vol. 2, World Sci., River Edge, N. J.

Sihvola, E. (1994), Coupling of spectral and vertical inversion in the analysis of stellar occultation data, *Geophys. Publ. 38*, Finn. Meteorol. Inst., Helsinki.

Steinbrecht, W., M. R. Gross, T. J. McGee, R. Neuber, P. von der Gathen, P. Wahl, U. Klein, and J. Langer (1999), Results of the 1998 Ny-Ålesund Ozone Measurements Intercomparison NAOMI, *J. Geophys. Res.*, *104*, 30,515–30,523.

Swartz, W. H., J.-H. Yee, R. J. Vervack Jr., S. A. Lloyd, and P. A. Newman (2002), Photochemical ozone loss in the Arctic as determined by MSX/UVISI stellar occultation observations during the 1999/2000 winter, *J. Geophys. Res.*, *107*(D20), 8296, doi:10.1029/2001JD000933.

Veiga, R. E., D. M. Cunnold, W. P. Chu, and M. P. McCormick (1995), Stratospheric Aerosol and Gas Experiments I and II comparisons with ozonesondes, *J. Geophys. Res.*, *100*, 9073–9090.

Vervack, R. J., Jr., J.-H. Yee, J. F. Carbary, and F. Morgan (2002), Atmospheric remote sensing using a combined extinctive and refractive stellar occultation technique: 3. Inversion method for refraction measurements, *J. Geophys. Res.*, *107*(D15), 4261, doi:10.1029/2001JD000796.

Vervack, R. J., Jr., J.-H. Yee, R. DeMajistre, and W. H. Schwartz (2003), Intercomparison of MSX/UVISI-derived ozone and temperature profiles with ground-based, SAGE II, HALOE, and POAM III data, *J. Geophys. Res.*, *108*(D22), 4697, doi:10.1029/2003JD003671.

World Meteorological Organization (WMO) (1988), Report of the International Ozone Trends Panel: 1988, *Rep. 18*, Global Ozone Res. and Monit. Proj., Geneva.

Yee, J.-H., et al. (2002), Atmospheric remote sensing using a combined extinctive and refractive stellar occultation technique: 1. Overview and proof-of-concept observations, *J. Geophys. Res.*, *107*(D14), 4213, doi:10.1029/2001JD000794.

M. Allaart and H. M. Kelder, Royal Netherlands Meteorological Institute, P. O. Box 201, NL-3730 AE De Bilt, Netherlands. (allaart@knmi.nl; kelder@knmi.nl)

S. B. Andersen, Department of Research and Development, Danish Meteorological Institute, Lyngbyvej 100, DK-2100 Copenhagen, Denmark. (sba@dmi.dk)

G. Bodeker, National Institute of Water and Atmospheric Research, Private Bag 50061, Omakau, Lauder, State Highway 85, Central Otago, New Zealand. (g.bodeker@niwa.co.nz)

I. Boyd, Department of Astronomy, University of Massachusetts, 619 Lederle Graduate Research Center, Amherst, MA 01003-9305, USA. (i.boyd@niwa.com)

G. O. Braathen, Norwegian Institute for Air Research, P. O. Box 100, Instituttveien 18, N-2027 Kjeller, Norway. (geir@nilu.no)

Y. Calisesi, Institute of Applied Physics, University of Bern, Sidlerstrasse 5, CH-3012 Bern, Switzerland. (yasmine.calisesi@issi.unibe.ch)

H. Claude, Meteorologisches Observatorium, Deutscher Wetterdienst, Albin-Schwaiger-Weg 10, D-82383 Hohenpeissenberg, Germany. (hans.claude@dwd.de)

V. Dorokhov, Central Aerological Observatory, Pervomayskaya str. 3, Dolgoprudny, Moscow Region 141700, Russia. (vdor@caomsk.mipt.ru)

M. Gil and M. Yela, Instituto Nacional de Técnica Aeroespacial, Calle Ajalvir km 4, E-28850 Torrejon de Ardoz, Spain. (gilm@inta.es; yelam@inta.es)

S. Godin-Beekmann, Service d'Aeronomie du CNRS, Université Pierre et Marie Curie, 4 Place Jussieu, F-75252 Paris Cedex 05, France. (sophie.godin@aero.jussieu.fr)

F. Goutail, Service d'Aeronomie du CNRS, B. P. 3, F-91371 Verrieres-le-Buisson, France. (fgoutail@aerov.jussieu.fr)

G. Hansen, Norwegian Institute for Air Research, Strandtorget 2B, P. O. Box 1245, N-9001 Tromsø, Norway. (ghh@nilu.no)

A. Karpetchko and T. Suortti, Finnish Meteorological Institute, Tähteläntie 62, FI-99600 Sodankylä, Finland. (alex.karpetchko@fmi.fi; tuomo.suortti@fmi.fi)

P. Keckhut, Institut Pierre Simon Laplace, Université de Versailles Saint-Quentin, B. P. 3, Reduit de Verrieres, F-91371 Verrieres-le-Buisson, France. (philippe.keckhut@aerov.jussieu.fr)

R. Koelemeijer, Netherlands Environmental Assessment Agency, RIVM, Postbus 1, NL-3720 BA Bilthoven, Netherlands. (robert.koelemeijer@rivm.nl)

B. Kois, Institute of Meteorology and Water Management, ul. Oleandrów 6, 00-629 Warszawa, Poland. (bogdan.kois@imgw.pl)

R. M. Koopman, European Space Agency, Via Galileio Galilei, CP 64, I-00044 Frascati, Italy. (rob.koopman@esa.int)

G. Kopp, Institut für Meteorologie und Klimaforschung, Forschungszentrum Karlsruhe, D-76021 Karlsruhe, Germany. (kopp@imk.fzk.de)

J.-C. Lambert, Space Aeronomy Institute of Belgium, 3 Avenue Circulaire, B-1180 Brussels, Belgium. (lambert@bira-iasb.oa.be)

T. Leblanc and I. S. McDermid, Table Mountain Observatory, Jet Propulsion Laboratory, 24490 Table Mountain Road, P.O. Box 367, Wrightwood, CA 92397-0367, USA. (leblanc@tmf.jpl.nasa.gov; mcdermid@tmf.jpl.nasa.gov)

Y. J. Meijer and D. P. J. Swart, Laboratory for Environmental Measurements (LVM), Environmental Risks and Safety Division, RIVM, P. O. Box 1, NL-3720 BA Bilthoven, Netherlands. (yasjka.meijer@rivm.nl; daan. swart@rivm.nl)

S. Pal, Department of Physics, York University, 4700 Keele Street, Toronto, Ontario, Canada M3J 2K1. (shiv@yorku.ca)

H. Schets, Royal Meteorological Institute of Belgium, Ringlaan 3, B-1180 Brussels, Belgium. (henk.schets@oma.be)

R. Stubi, MeteoSwiss, Station aérologique, Les Invuardes, CH-1530 Payerne, Switzerland. (rsi@meteoswiss.ch)

G. Visconti, Department of Physics, University of L'Aquila, I-67010, Coppito (L'Aquila), Italy. (guido.visconti@aquila.infn.it)

P. von der Gathen, Alfred Wegener Institute for Polar and Marine Research, Telegrafenberg A43, D-14473 Potsdam, Germany. (gathen@awi-potsdam.de)